

1 **A mosaic of phytoplankton responses across Patagonia, the southeast Pacific and**  
2 **southwest Atlantic Oceans to ash deposition and trace metal release from the Calbuco**  
3 **volcanic eruption in 2015**

4 Maximiliano J. Vergara-Jara<sup>1,2</sup>, Mark J. Hopwood<sup>3\*</sup>, Thomas J. Browning<sup>3</sup>, Insa Rapp<sup>4</sup>,  
5 Rodrigo Torres<sup>2,5</sup>, Brian Reid<sup>5</sup>, Eric P. Achterberg<sup>3</sup>, José Luis Iriarte<sup>2,6</sup>.

6  
7 <sup>1</sup>Programa de Doctorado en Ciencias de la Acuicultura, Universidad Austral de Chile, Puerto  
8 Montt, Chile.

9 <sup>2</sup>Instituto de Acuicultura & Centro de Investigación Dinámica de Ecosistemas Marinos de  
10 Altas Latitudes - IDEAL, Universidad Austral de Chile, Puerto Montt, Chile.

11 <sup>3</sup>GEOMAR, Helmholtz Centre for Ocean Research, 24148 Kiel, Germany.

12 <sup>4</sup>Department of Biology, Dalhousie University, Halifax, Nova Scotia, Canada

13 <sup>5</sup>Centro de Investigación en Ecosistemas de la Patagonia (CIEP), Coyhaique, Chile.

14 <sup>6</sup>COPAS-Sur Austral, Centro de Investigación Oceanográfica en el Pacífico Sur-Oriental  
15 (COPAS), Universidad de Concepción, Concepción, Chile.

16  
17 Key words: volcanic ash, iron, Fe(II), phytoplankton, carbonate chemistry, Reloncaví Fjord

18 Corresponding author\*: [mhopwood@geomar.de](mailto:mhopwood@geomar.de)

19  
20  
21  
22  
23  
24  
25  
26  
27  
28  
29  
30  
31  
32  
33  
34  
35  
36  
37

38 **Abstract**

39 Following the eruption of the Calbuco volcano in April 2015, an extensive ash plume spread  
40 across northern Patagonia and into the southeast Pacific and southwest Atlantic Oceans. Here  
41 we report on field surveys conducted in the coastal region receiving the highest ash load  
42 following the eruption (Reloncaví Fjord). The fortuitous location of a long-term monitoring  
43 station in Reloncaví Fjord provided data to evaluate inshore phytoplankton bloom dynamics  
44 and carbonate chemistry during April-May 2015. Satellite derived chlorophyll-a  
45 measurements over the ocean regions affected by the ash plume in May 2015 were obtained  
46 to determine the spatial-temporal gradients in offshore phytoplankton response to ash.  
47 Additionally, leaching experiments were performed to quantify the release from ash into  
48 solution of total alkalinity, trace elements (dissolved Fe, Mn, Pb, Co, Cu, Ni and Cd) and  
49 major ions ( $F^-$ ,  $Cl^-$ ,  $SO_4^{2-}$ ,  $NO_3^-$ ,  $Li^+$ ,  $Na^+$ ,  $NH_4^+$ ,  $K^+$ ,  $Mg^{2+}$ ,  $Ca^{2+}$ ). Within Reloncaví Fjord,  
50 integrated peak diatom abundances during the May 2015 austral bloom were approximately  
51 2-4 times higher than usual (up to  $1.4 \times 10^{11}$  cells  $m^{-2}$ , integrated to 15 m depth), with the  
52 bloom intensity perhaps moderated due to high ash loadings in the two weeks following the  
53 eruption. Any mechanistic link between ash deposition and the Reloncaví diatom bloom can  
54 however only be speculated on due to the lack of data immediately preceding and following  
55 the eruption. In the offshore southeast Pacific, a short duration phytoplankton bloom  
56 corresponded closely in space and time to the maximum observed ash plume, potentially in  
57 response to Fe-fertilization of a region where phytoplankton growth is typically Fe-limited  
58 at this time of year. Conversely, no clear fertilization on the same time-scale was found in  
59 the area subject to an ash plume over the southwest Atlantic where the availability of fixed  
60 nitrogen is thought to limit phytoplankton growth. This was consistent with no significant  
61 release of fixed nitrogen ( $NO_x$  or  $NH_4$ ) from Calbuco ash.

62

63 In addition to release of nanomolar concentrations of dissolved Fe from ash suspended in  
64 seawater, it was observed that low loadings ( $< 5 \text{ mg L}^{-1}$ ) of ash were an unusually prolific  
65 source of Fe(II) into chilled seawater (up to  $1.0 \text{ } \mu\text{mol Fe g}^{-1}$ ), producing a pulse of Fe(II)  
66 typically released mainly during the first minute after addition to seawater. This release  
67 would not be detected, either as Fe(II) or dissolved Fe, following standard leaching protocols  
68 at room temperature. A pulse of Fe(II) release upon addition of Calbuco ash to seawater made  
69 it an unusually efficient dissolved Fe source. The fraction of dissolved Fe released as Fe(II)  
70 from Calbuco ash (~18-38%) was roughly comparable to literature values for Fe released  
71 into seawater from aerosols collected over the Pacific Ocean following long range  
72 atmospheric transport.

73 **1. Introduction**

74 Volcanic ash has long been considered a large, intermittent source of trace metals to the ocean  
75 (Frogner et al., 2001; Sarmiento, 1993; Watson, 1997) and its deposition is now deemed a  
76 sporadic generally low-macronutrient, high-micronutrient supply mechanism (Ayris and  
77 Delmelle, 2012; Jones and Gislason, 2008; Lin et al., 2011). As volcanic ash can be a  
78 regionally significant source of allochthonous inorganic material to affected water bodies,  
79 volcanic eruptions have the potential to dramatically change light availability, the carbonate  
80 system, properties of sinking particles and ecosystem dynamics (Hoffmann et al., 2012;  
81 Newcomb and Flagg, 1983; Stewart et al., 2006). Surveys directly underneath the ash plume  
82 from the 2010 eruption of Eyjafjallajökull (Iceland) over the North Atlantic found, among  
83 other biogeochemical perturbations, high dissolved Fe (dFe) concentrations of up to 10 nM  
84 in affected surface seawater (Achterberg et al., 2013) which could potentially result in  
85 enhanced primary production. The greatest potential positive effect of ash deposition on  
86 marine productivity would generally be expected in high-nitrate, low-chlorophyll (HNLC)  
87 areas of the ocean (Hamme et al., 2010; Mélançon et al., 2014), where low Fe concentrations  
88 are a major factor limiting primary production (Martin et al., 1990; Moore et al., 2013).  
89 Special interest is therefore placed on the ability of volcanic ash to release dFe, and other  
90 bio-essential trace metals such as Mn (Achterberg et al., 2013; Browning et al., 2014;  
91 Hoffmann et al., 2012), into seawater. In contrast, apart from inducing light limitation, there  
92 are several adverse effects of ash deposition on aquatic organisms. These include metal  
93 toxicity (Ermolin et al., 2018), particularly under high dust loading (Hoffmann et al., 2012),  
94 and the ingestion of ash particles by filter feeders, phagotrophic organisms or fish (Newcomb  
95 and Flagg, 1983; Wolinski et al., 2013). Transient shifts to low pH have also been reported  
96 in some, but not all, ash leaching experiments and in some freshwater bodies following

97 intense ash deposition events, suggesting that significant ash deposition on weakly buffered  
98 aquatic environments can also impact and perturb their carbonate system (Duggen et al.,  
99 2010; Jones and Gislason, 2008; Newcomb and Flagg, 1983). The greatest negative impact  
100 of ash on primary producers would therefore be expected closest to the source where the ash  
101 loading is highest and in areas where macronutrients or light, rather than trace elements, limit  
102 primary production.

103

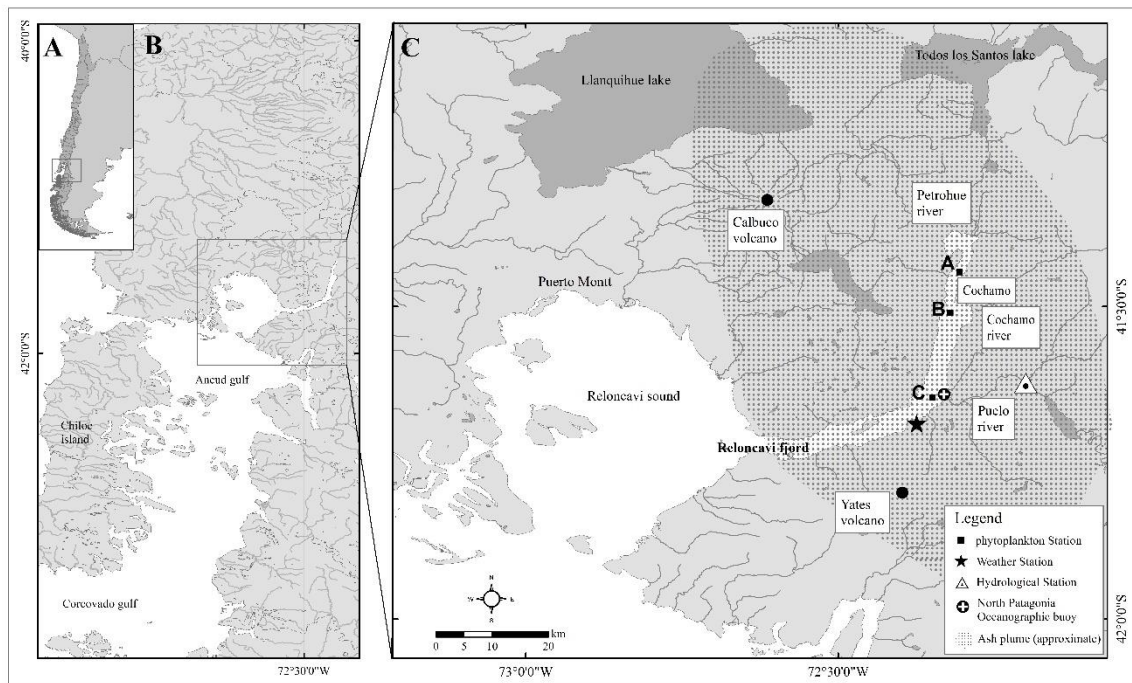
104 In contrast to the 2010 Eyjafjallajökull plume over the North Atlantic, the 2015 ash plume  
105 over the region from the Calbuco eruption (northern Patagonia, Chile) was predominantly  
106 deposited over an inshore and coastal region (Romero et al., 2016) (Fig. 1). This led to visible  
107 high ash loadings in affected surface waters in the weeks after the eruption (Fig. 2), providing  
108 a case study for a concentrated ash deposition event in a coastal system; Reloncaví Fjord,  
109 which is the northernmost fjord of Patagonia. It receives the direct discharge from three major  
110 rivers, creating a highly stratified and productive fjord system in terms of both phytoplankton  
111 biomass and aquaculture production of mussels (González et al., 2010; Molinet et al., 2017;  
112 Yevenes et al., 2019). Here we combine in situ observations from moored arrays which were  
113 fortuitously deployed in Reloncaví Fjord (Vergara-Jara et al., 2019), with satellite-derived  
114 chlorophyll data for offshore regions subject to ash deposition, and leaching experiments  
115 carried out on ash collected from the fjord region, to investigate the inorganic consequences  
116 of ash addition to natural waters. We thereby evaluate the potential positive and negative  
117 effects of ash from the 2015 Calbuco eruption on marine phytoplankton in three geographical  
118 regions; Reloncaví Fjord and the areas of the SE Pacific and SW Atlantic Oceans beneath  
119 the most intense ash plume.

120

121 **2. Materials and methods**

122 **2.1. Study area**

123 The Calbuco volcano (Fig. 1) is located in a region with large freshwater reservoirs and in  
124 close proximity to Reloncaví Fjord. The predominant bedrock type is andesite (López-  
125 Escobar et al., 1995). Reloncaví Fjord is 55 km long and receives freshwater from 3 main  
126 rivers, the Puelo, Petrohué, and Cochamó, with mean stream flows of  $650 \text{ m}^3 \text{ s}^{-1}$ ,  $350 \text{ m}^3 \text{ s}^{-1}$   
127 and  $100 \text{ m}^3 \text{ s}^{-1}$ , respectively (León-Muñoz et al., 2013). River discharge strongly influences  
128 seasonal patterns of primary production across the region, supplying silicic acid and strongly  
129 stratifying the water column (Castillo et al., 2016; González et al., 2010; Torres et al., 2014).  
130 Seasonal changes in light availability rather than macronutrient supply are thought to control  
131 marine primary production across the Reloncaví region with high marine primary production  
132 ( $>1 \text{ g C m}^{-2} \text{ day}^{-1}$ ) throughout austral spring, summer and early autumn (González et al.,  
133 2010).



134

135 Figure 1. The Calbuco region showing the location of Reloncaví Fjord, 3 major rivers  
136 (Petrohué, Cochamó and Puelo) discharging into the fjord, the 3 stations (black squares; A,  
137 B and C) used to assess changes in phytoplankton abundance following the eruption, a  
138 hydrological station that monitors Puelo river flow, a weather station and the location of a  
139 long-term mooring within the fjord. The approximate extent of the ash plume in the week  
140 following the first eruption is illustrated, as estimated in technical reports issued by the  
141 Servicio Nacional de Geología y Minería (Chile).

142

143 On 22 April 2015 the Calbuco volcano erupted after 54 years of dormancy. Two major  
144 eruption pulses lasted <2 hours on 22 April and 6 hours on 23 April, releasing a total volume  
145 of 0.27 km<sup>3</sup> ash which was projected up to 20 km height above sea level (Van Eaton et al.,  
146 2016; Romero et al., 2016). Ash layers of several cm thick were deposited mainly to the NE  
147 of the volcano in subsequent days (Romero et al., 2016). A smaller eruption occurred on 30  
148 April projecting ash 4-5 km above sea level which was then mainly deposited south of the  
149 volcano. Smaller volumes of ash were released semi-continuously for three weeks after the  
150 main eruption, leading to intermittent ash deposition events. Fortuitously, as part of a long-  
151 term deployment, an ocean acidification buoy in the middle of Reloncaví Fjord (Vergara-  
152 Jara et al., 2019) and an associated meteorological station close to the volcano (Fig. 1) were  
153 well placed to assess the impact of ash deposition immediately after the eruption. To  
154 complement data from these facilities, after the regional evacuation order was removed,  
155 weekly sampling campaigns were conducted in the fjord commencing one week after the  
156 eruption. The Chilean Geological-mining Survey (Servicio Nacional de Geología y Minería,  
157 SERNAGEOMIN) produced daily technical reports including the estimated area of ash  
158 dispersion (<http://sitiohistorico.sernageomin.cl/volcan.php?pagina=4&iId=3>). This

159 information was used to create a reference aerial extent of ash deposition for the week after  
160 the eruption (Fig. 1, C). This approximation represents a full week of coverage for this  
161 dynamic feature.

162

## 163 **2.2. Ash samples – trace metal leaching experiments**

164 On 6 May (2015, Cochamó, Chile, approximately 30 km from the volcano) after the third,  
165 and smallest, eruptive pulse of ash from the Calbuco volcano (Fig. 2, A), and with the volcano  
166 still emitting material, ash was collected using a plastic tray wrapped with plastic sheeting  
167 (40 × 94 cm). The plasticware was left outside for 24 hours until sufficient ash (~500 g) was  
168 collected to provide a bulk sample. Ambient weather over the period of ash collection, and  
169 the preceding day, was dry (no precipitation). The collected ash was double sealed in low  
170 density polyethylene (LDPE) plastic bags and stored in the dark. A sub-sample was analyzed  
171 for particle size using a Mastersizer 2000 at The University of Chile.

172 Ash may affect in situ phytoplankton dynamics in several ways, for example via moderating  
173 the carbonate system, macronutrient availability and/or micronutrient availability. As  
174 micronutrient (e.g. Fe and Mn) availability is expected to be the main chemical mechanism  
175 via which phytoplankton dynamics in the offshore marine environment could be affected, we  
176 primarily focus our investigation on the release of dissolved trace metals from ash in  
177 seawater. Yet to rule out other potential affects, we also conduct complementary leaches to  
178 assess the significance of changes to total alkalinity and macronutrient availability (Table 1).  
179 For trace metal leaches, a variety of methods have been used in the literature (Duggen et al.,  
180 2010; Witham et al., 2005) depending on the purpose of specific studies. De-ionized water  
181 leaches with ash loadings that are high in an offshore environmental context are preferable



182 for intercomparison studies. The trace metals released under such conditions are however  
183 difficult to compare quantitatively to metal exchange processes in the ambient marine  
184 environment, especially for elements such as Fe where solubility is strongly influenced by  
185 pH, salinity and the nature of dissolved organic carbon present (Baker and Croot, 2010). For  
186 prior work conducted specifically using volcanic ash in seawater, 3 main methods have been  
187 employed: suspension experiments followed by analysis of the leachate, flow-through  
188 reactors, and continuous voltammetric determination of dFe concentrations in situ during  
189 suspension experiments (Sup. Table 1). The most commonly used ash:solute ratio in prior  
190 seawater experiments is 1:400 (g:mL), with leach lengths varying from 15 minutes to 24  
191 hours (Sup. Table 1). Conversely, incubation experiments designed to test the response of  
192 marine phytoplankton to ash deposition have used lower ash:solute ratios of 1:400 to 1:10<sup>7</sup>  
193 which are based on estimates of the ash loading expected to be mixed within the offshore  
194 surface mixed layer underneath ash plumes (Browning et al., 2014; Hoffmann et al., 2012).  
195 Existing data suggests that ash:solute ratio is not a major factor in determining the release  
196 behavior of Fe from ash, however this is acknowledged to be difficult to assess due to other  
197 differences between experimental setups used to date (Duggen et al., 2010). Both the age of  
198 particles since collection and the organic carbon content of seawater are however known to  
199 be critical factors influencing the exchange of Fe, and other trace elements, following any  
200 aerosol deposition into seawater (Baker and Croot, 2010; Duggen et al., 2010). Whilst UV-  
201 treatment of seawater has been used in some experiments (to remove a large part of any  
202 natural organic ligands present, Duggen et al., 2007; Jones and Gislason, 2008), and a strong  
203 synthetic organic ligand added in others (to impede dissolved Fe precipitation, Duggen et al.,  
204 2007; Olgun et al., 2011; Simonella et al., 2015), to improve reproducibility and  
205 standardisation, these steps are not well suited specifically for investigating the release of

206 Fe(II) from ash. Herein we therefore adopt ash:solute ratios comparable to the lower end of  
207 the range used in leaching experiments and comparable to the range used in incubation  
208 experiments. Seawater was used after prolonged storage in the dark (to reduce biological  
209 activity to low background levels) and without UV treatment (to maintain an environmentally  
210 relevant level of natural organic material in solution). A short leaching time (10 minutes +  
211 filtration) was adopted to minimize bottle effects and recognising that most prior work  
212 suggests a large fraction of Fe release occurs on short timescales (minutes), followed by more  
213 gradual changes on timescales of hours to days (Duggen et al., 2007; Frogner et al., 2001;  
214 Jones and Gislason, 2008).

215 A variety of leaches were conducted in de-ionized water, brackish (fjord) water or offshore  
216 South Atlantic seawater (Table 1) with the choice of leaching conditions based on the  
217 expected environmental significance in different water masses. Offshore oligotrophic  
218 seawater for incubation experiments was collected from an underway transect of the mid-  
219 South Atlantic (across 40° S) using a towfish and trace metal clean tubing in a 1 m<sup>3</sup> high  
220 density polyethylene tank which had been pre-rinsed with 1 M HCl. This water was stored  
221 in the dark for >12 months prior to use in leaching experiments and was filtered  
222 (AcroPak1000 capsule 0.8/0.2 µm filters) when subsampling a batch for use in all leaching  
223 experiments. All labware for trace metal leaching experiments was pre-cleaned with Mucosal  
224 and 1 M HCl. 125 ml LDPE bottles (Nalgene) for trace metal leach experiments were pre-  
225 cleaned using a 3-stage procedure with three de-ionized water (Milli-Q, Millipore,  
226 conductivity 18.2 MΩ cm<sup>-1</sup>) rinses after each stage (3 days in Mucosal, 1 week in 1 M HCl,  
227 1 week in 1 M HNO<sub>3</sub>).

228 Leach experiments were conducted by adding a pre-weighed mass of ash into 100 ml South

229 Atlantic Seawater, gently mixing the suspension for 10 minutes, and then syringe filtering  
230 the suspension (0.2  $\mu\text{m}$ , polyvinylidene fluoride, Millipore). Eight different ash loadings  
231 from 2-50  $\text{mg L}^{-1}$  were used, selected to be environmentally relevant and comparable to prior  
232 incubation experiments, with each treatment run in triplicate. Samples for dissolved trace  
233 metals (Fe, Cd, Pb, Ni, Cu, Co and Mn) were acidified within 1 day of collection by the  
234 addition of 140  $\mu\text{L}$  concentrated HCl (UPA grade, ROMIL) and analysed by inductively  
235 coupled plasma mass spectroscopy following preconcentration exactly as per Rapp et al.,  
236 (2017).

237 Leach experiments specifically to measure Fe(II) release were conducted in a similar manner  
238 but in cold seawater with continuous in-line analysis (5-7°C see Sup. Table 2) due to the  
239 rapid oxidation rate of Fe(II) at room temperature ( $\sim 21^\circ\text{C}$ ), which makes accurate  
240 measurement of Fe(II) concentrations challenging (Millero et al., 1987). For these  
241 experiments, a pre-weighed mass of ash was added to 250 ml South Atlantic seawater and  
242 manually shaken for approximately one minute, using an expanded loading range from 0.2-  
243 4000  $\text{mg L}^{-1}$ . Fe(II) was measured via flow injection analysis using luminol  
244 chemiluminescence (Jones et al., 2013) without pre-concentration or filtration. The inflow  
245 line feeding the flow injection apparatus was positioned inside the ash suspension  
246 immediately after mixing and measurements begun thereafter at 2 minutes resolution.  
247 Reported mean values ( $\pm$  standard deviation) are determined from the Fe(II) concentrations  
248 measured 2-30 minutes after adding ash into solution. Calibrations were run daily using  
249 standard additions of 0.2-10 nM Fe(II) to aged South Atlantic seawater at the same  
250 temperature with integrated peak area used to construct calibration curves. Following each  
251 leaching experiment the apparatus was rinsed with 0.1 M HCl (reagent grade) followed by

252 flushing with de-ionized water to ensure the removal of ash particles. Blank measurements  
253 before/after Fe(II) measurements from experiments with different ash loadings verified that  
254 there was no discernable interference from ash particles in the Fe(II) flow-through  
255 measurements. Fe(II) leaches were conducted 2 weeks, 4 months and 9 months after the  
256 eruption. Fe(II) leaches 2 weeks after the eruption were run for 30 minutes. Fe(II) leaches  
257 after 4 or 9 months were run for 1 hour to further investigate the temporal development of  
258 Fe(II) concentration. The trace metal leach experiments (above) were conducted at the same  
259 time as the first Fe(II) incubation experiments (2 weeks after ash collection).

260 For trace metal leaches, the initial (mean  $\pm$  standard deviation) dissolved trace metal  
261 concentrations were deducted from the final concentrations, in order to calculate the net  
262 change as a result of ash addition. For Fe(II) measurements, background levels of Fe(II) were  
263 below detection ( $<0.1$  nM) and so no deduction was made.

### 264 **2.3 Ash samples – de-ionized and brackish water leaching experiments**

265 Fresh brackish sub-surface water from the Patagonia study region was obtained from the  
266 Aysén Fjord, at Ensenada Baja (45°21'S: 72°40'W, salinity 16.3), close to the Coyhaique  
267 laboratory (Aysén region, Chile) and free from the influence of ash from the 2015 eruption.  
268 The oceanographic conditions in these waters are similar to the adjacent Reloncaví fjord  
269 (Cáceres et al., 2002). De-ionized water, along with the Aysén fjord brackish water, were  
270 used for leaching experiments using two size fractions of ash following the general  
271 recommendations of Duggen et al., (2010) and Witham et al., (2005) to consider the effects  
272 of different size fractions and leachates. Leaches were conducted in 50 ml LDPE bottles filled  
273 with either 40 ml brackish or DI-water with 4 replicates of each treatment. Bottles were

274 incubated inside a mixer at room temperature after the addition of 0.18 g ash, using two ash  
275 size fractions (<63  $\mu\text{m}$  and 250-1000  $\mu\text{m}$ ) which were separated using sieves (ASTM e-11  
276 specification, W.S. Tyler). The mass distribution of the ash as determined by sieving was  
277 4.54% >2360  $\mu\text{m}$ ; 6.85% <2360  $\mu\text{m}$  and >1000  $\mu\text{m}$ ; 31.12% <1000  $\mu\text{m}$  and >250  $\mu\text{m}$ ;  
278 24.14% <250  $\mu\text{m}$  and >125  $\mu\text{m}$ ; 18.04% <125  $\mu\text{m}$  and >63  $\mu\text{m}$ ; 15.31% <63  $\mu\text{m}$ . The  
279 dominant size fraction by mass was thereby the 250-1000  $\mu\text{m}$  fraction which was analyzed  
280 in addition to the finest fraction (<63  $\mu\text{m}$ ) with the greatest surface area to mass ratio. The  
281 sampling times were at time zero (defined as just after the addition of the ash and a few  
282 minutes of mixing), 2 h and 24 h later. Leaching experiments conducted with brackish water  
283 were analyzed for total alkalinity ( $A_T$ ) via a potentiometric titration using reference standards  
284 (Haraldsson et al., 1997) ensuring a reproducibility of <2  $\mu\text{mol/kg}$ . For the de-ionized water  
285 leaching experiment,  $A_T$  was analyzed by titration of unfiltered 5 ml subsamples to a pH 4.5  
286 endpoint (Bromocresol Green/Methyl Red) using a Dosimat (Metrohm Inc) and 0.02 N  
287  $\text{H}_2\text{SO}_4$  titrant. Alkalinity was calculated as  $\text{CaCO}_3$  equivalents following APHA (American  
288 Public Health Association) 2005-Methods 2320 (2320 Alkalinity, titration method).  
289 Additional 5 ml subsamples were filtered, stored at 4°C and analyzed within 3 days for major  
290 ions ( $\text{F}^-$ ,  $\text{Cl}^-$ ,  $\text{SO}_4^{2-}$ ,  $\text{NO}_3^-$ ,  $\text{Li}^+$ ,  $\text{Na}^+$ ,  $\text{NH}_4^+$ ,  $\text{K}^+$ ,  $\text{Mg}^{2+}$ ,  $\text{Ca}^{2+}$ ) using a Dionex™ 5000 Ion  
291 Chromatography system with Eluent Generation (APHA). All measurements were then  
292 corrected for initial water concentrations prior to ash addition. Saturation indices for species  
293 in solution following leaching from <63  $\mu\text{m}$  ash particles were obtained from the MINTEQA  
294 3.1. IAP Ion Activity Product chemical equilibrium model (see Sup. Table 6).

295 Table 1. Summary of different leaching experiments and samples.

Ash/ particle source	De-ionized water leaches	Brackish (fjord) water	South Atlantic seawater	Number of replicates
Calbuco ash, sieved <63 $\mu\text{m}$	Total alkalinity, ion and macronutrients	Total alkalinity	-	4
Calbuco ash, sieved 250-1000 $\mu\text{m}$	Total alkalinity, ion and macronutrients	Total alkalinity	-	4
Calbuco ash, unsieved	-	-	Trace metals, Fe(II)	3 for trace elements, 1 time series for Fe(II)

296 **2.4 Environmental data – continuous Reloncaví Fjord monitoring**

297 High temporal resolution (hourly) in situ measurements were taken in the Reloncaví fjord  
298 (Fig. 1 C, North Patagonia Oceanographic Buoy) at 3 m depth using SAMI sensors that  
299 measured spectrophotometric CO<sub>2</sub> and pH (DeGrandpre et al., 1995; Seidel et al., 2008)  
300 (Sunburst Sensors, LLC), and an SBE 37 MicroCAT CTD-ODO (SeaBird Electronics) for  
301 temperature, conductivity, depth and dissolved O<sub>2</sub>, as per Vergara-Jara et al., (2019). Sensor  
302 maintenance and quality control is described by Vergara-Jara et al., (2019). The error in pCO<sub>2</sub>  
303 concentrations is estimated to be at most 5% which arises mainly due to a non-linear sensor  
304 response and reduced sensitivity at high pCO<sub>2</sub> levels >1500 ppm (DeGrandpre et al., 1999).  
305 The SAMI-pH instruments used an accuracy test instead of a calibration procedure (Seidel  
306 et al., 2008). With the broad pH and salinity range found in the fjord, pH values are subject  
307 to a maximum error of  $\pm 0.02$  (Mosley et al., 2004).

308 A meteorological station (HOBO-U30, Fig. 1) measured air temperature, solar radiation,

309 wind speed and direction, rainfall, and barometric pressure every 5 minutes. Puelo River  
310 streamflow was obtained from the Carrera Basilio hydrological station (Fig. 1), run by  
311 Dirección General de Aguas de Chile (<http://snia.dga.cl/BNAConsultas/reportes>).

## 312 **2.5 Field surveys in Reloncaví Fjord post eruption**

313 During May 2015, weekly field campaigns were undertaken in the Reloncaví Fjord.  
314 Phytoplankton samples were collected at 3 depths (1, 5 and 10 m) for taxonomic  
315 characterization and abundance determination at 3 stations (A, B and C; Fig. 1) using a 5 L  
316 Go-Flo bottle. Samples for cell-counts were stored in clear plastic bottles (300 mL) and  
317 preserved in a Lugol iodine solution. From each sample, a 10 mL subsample was placed in a  
318 sedimentation chamber and left to settle for 16 hr. The complete chamber bottom was  
319 scanned at 200× to enumerate the organisms and the result was expressed as number of  
320 phytoplankton cells per L of seawater (Hasle, 1978). Phytoplankton were identified to genus  
321 or species level, when possible, and divided into diatoms and dinoflagellates. Samples were  
322 analyzed using an Olympus CKX41 inverted phase contrast microscope and the Utermöhl  
323 method (Utermöhl, 1958). The phytoplankton community composition was then statistically  
324 analyzed in R (RStudio V 1.2.5033) using general linear models in order to find statistically  
325 significant differences between dates and group abundances. Additionally, as part of a long-  
326 term monitoring program at station C (Fig. 1), chlorophyll-a samples were retained from 6  
327 depths (1, 3, 5, 7, 10 and 15 m) on 6 occasions during March-May 2015. Chlorophyll-a was  
328 determined by fluorometry after filtering 250 ml of sampled water through GFF filters  
329 (Whatman) as per Welschmeyer (1994). Two additional profiles close to Station C were  
330 obtained from Yevenes et al., (2019). Integrated chlorophyll-a ( $\text{mg m}^{-2}$ ) and diatom  
331 abundance ( $\text{cells m}^{-2}$ ) were determined to 15 m depth. Chlorophyll-a within Reloncaví Fjord

332 is invariably concentrated in the upper ~10 m (González et al., 2010; Yevenes et al., 2019)  
333 and thus, for comparison to prior reported data integrated to 10 m, only a small difference is  
334 anticipated. For all profiles considered herein, there is a 20% difference between integrating  
335 to 10 m or 15 m depth.

## 336 **2.6 Satellite data**

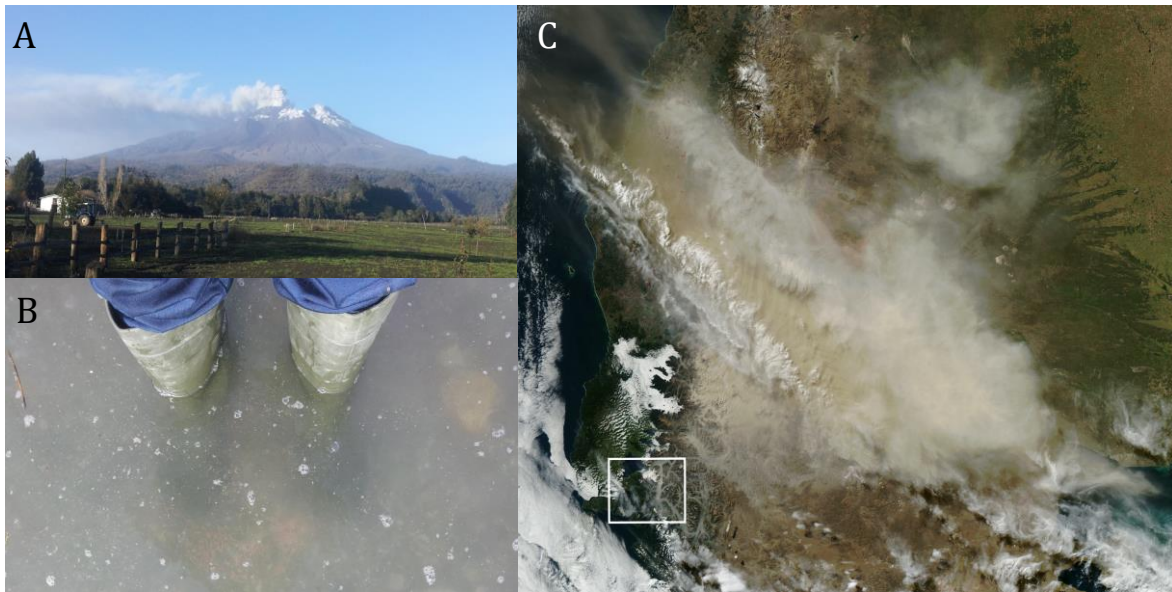
337 Daily, 4 km resolution chlorophyll-a images from the MODIS Aqua sensor (OCI algorithm;  
338 Hu et al., 2012) were downloaded from the NASA Ocean Color website  
339 (<https://oceancolor.gsfc.nasa.gov>) for the period 4 April 2015–2 May 2015. As the UV  
340 Aerosol Index largely reflects strongly UV-absorbing (dust) aerosols (Torres et al., 2007),  
341 this was used as a proxy for the spatial extent and loading of the ash plume. The UV aerosol  
342 index product from the Ozone Monitoring Instrument (OMI) on the EOS-Aura was  
343 downloaded for the same time period. Daily images were composited into 5-day mean  
344 averages.

## 345 **3. Results**

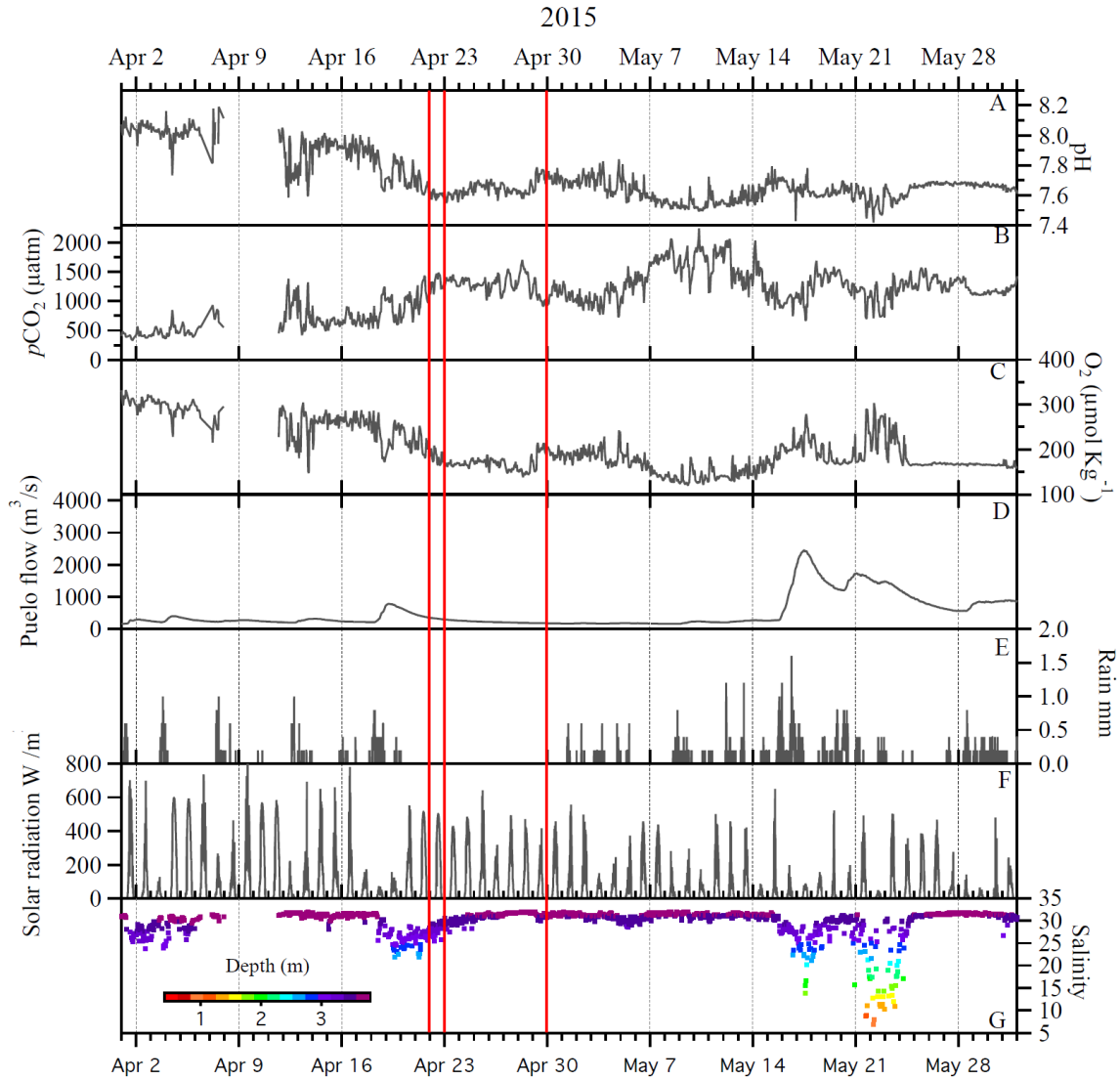
### 346 **3.1 In situ observations**

347 The Calbuco ash plume reached up to 20 km height and was dispersed hundreds of kilometers  
348 across Patagonia and the Pacific and Atlantic Oceans (Fig. 2) (Van Eaton et al., 2016;  
349 Reckziegel et al., 2016; Romero et al., 2016). The ash loading in water bodies near the cone  
350 was visually observed to be high, especially near the Petrohué river catchment that drains  
351 into the head of the Reloncaví fjord. This ash loading into the fjord was clearly visible on 6  
352 May 2015 when ash samples were collected for leaching experiments (Fig. 2).





354 Figure 2. A Calbuco volcano ash plume 6 May 2015. B Reloncaví Fjord water with atypical  
355 high turbidity due to the ash loading, Cochamó town 6 May. C Ash cloud visible on MODIS  
356 Aqua satellite from the NASA Earth Observatory, 23 April  
357 ([http://earthobservatory.nasa.gov/NaturalHazards/view.php?id=85767&eocon=home&eocon=](http://earthobservatory.nasa.gov/NaturalHazards/view.php?id=85767&eocon=home&eocon=home)  
358 [nh](http://earthobservatory.nasa.gov/NaturalHazards/view.php?id=85767&eocon=home&eocon=home)). The highlighted box in C corresponds to Fig. 1 C.



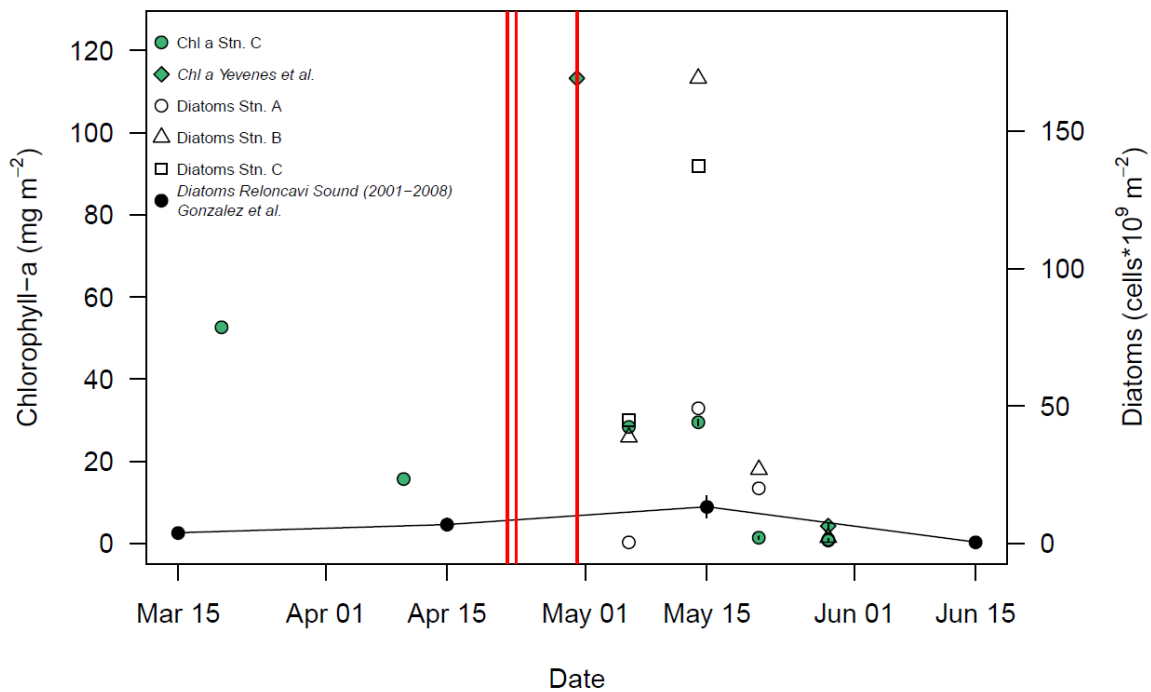
359

360 Figure 3. Continuous data from the Reloncaví Fjord mooring and nearby hydrological and  
 361 weather stations for April-May 2015. The vertical red lines mark the eruption dates. All  
 362 locations are marked in Fig 1. Carbonate chemistry and salinity data from Vergara-Jara et  
 363 al., (2019). Wind and tidal mixing caused small changes in the depth of the sensors which  
 364 are shown alongside the salinity data.

365

366 Carbonate chemistry data from the Reloncaví Fjord mooring demonstrated that pH declined  
367 and pCO<sub>2</sub> increased in the week prior to the first eruption (22 April, Fig. 3). Oxygen and pH  
368 reached a minimum and pCO<sub>2</sub> a maximum during the time period 7-14 May, which indicates  
369 a state of high respiration. In this stratified environment, the brackish fjord surface layer has  
370 generally low pH, high pCO<sub>2</sub> with seasonal changes in salinity and respiration leading to a  
371 large annual range of pCO<sub>2</sub> and pH (Vergara-Jara et al., 2019). The depth of the sensors  
372 varied temporally due to changes in tides and river flow. This accounts for some of the  
373 variation in measured salinity due to the strong salinity gradient with depth in the brackish  
374 surface waters (Fig. 3). Any changes to pCO<sub>2</sub> or pH occurring as a direct result of the  
375 eruptions, or associated ash deposition, are therefore challenging to distinguish from  
376 background variation due to short-term (intra-day) or seasonal shifts in the carbonate system  
377 which are pronounced in this dynamic and strongly freshwater influenced environment (Fig.  
378 3). Freshwater discharge from the Puelo increased sharply from 16 May which is an annually  
379 recurring event (González et al., 2010).

### 380 **3.2 Phytoplankton in Reloncaví fjord post-eruption**



381

382 Figure 4. Changes in integrated (0-15 m) diatom abundance and chlorophyll-a for Reloncaví  
 383 Fjord in April-May 2015. Locations as per Fig. 1, the eruption dates are marked with red  
 384 lines. Historical diatom data from Reloncaví Sound (2001-2008, integrated to 10 m depth,  
 385 mean  $\pm$  standard error, González et al., 2010) and additional chlorophyll data from 2015  
 386 ('Station 3' from Yevenes et al., 2019, approximately corresponding to Station C herein) are  
 387 also shown.

388

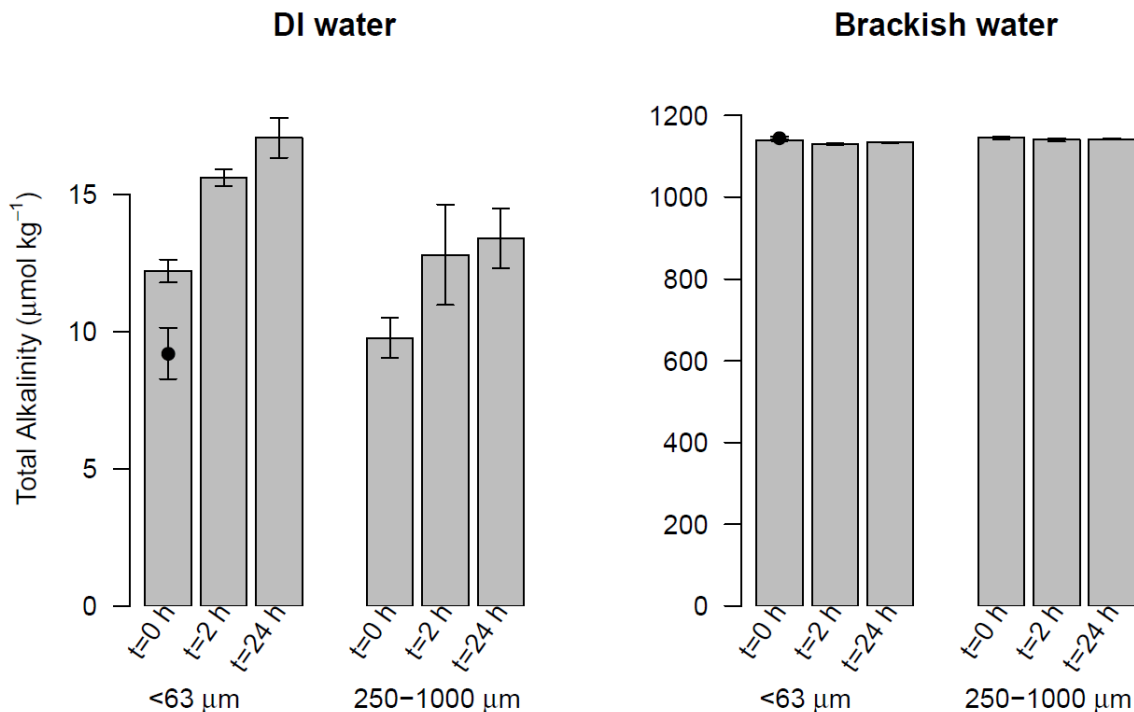
389 Phytoplankton abundances observed in May 2015 within Reloncaví Fjord were assessed by  
 390 diatom cell counts and chlorophyll-a concentrations (Sup. Table 3) and were proportionate  
 391 to, or higher than, those previously observed in the region (Fig. 4). When comparing  
 392 observations to prior data from González et al., (2010) it should be noted that there is a slight  
 393 depth discrepancy (earlier work was integrated to 10 m depth rather than 15 m herein). Yet  
 394 as the phytoplankton bloom is overwhelmingly present within the upper 10 m these data do

395 provide a useful comparison. Diatom abundance integrated to 15 m depth peaked at Stations  
396 B and C around 14 May, with notably lower abundances at the innermost station A (Fig. 4).  
397 The highest measured chlorophyll-a concentrations were on 30 April at Station C, then  
398 chlorophyll-a values declined to much lower concentrations in late May which is expected  
399 from patterns in regional primary production (González et al., 2010). No measurements were  
400 available for 10-30 April 2015 (Fig. 4) and thus it is not possible to determine the timing of  
401 the onset of the austral autumn phytoplankton bloom with respect to the volcanic eruptions  
402 from the available chlorophyll-a or diatom data. Within this time period, the mooring at  
403 Station C (Fig. 3) however did record a modest increase in pH and O<sub>2</sub> from 28-29 April,  
404 during a time period when river discharge and salinity were stable, which could be indicative  
405 of the autumn phytoplankton bloom onset.

406

### 407 **3.3 Total alkalinity and macronutrients in leach experiments**

408 Size analysis of the collected ash determined a mean particle diameter of 339 µm. Small ash-  
409 particles (<63 µm) resulted in minor, or no significant, changes to A<sub>T</sub> in brackish fjord waters  
410 (Fig. 5). With larger ash-particles (250-1000 µm) no effect was evident. Conversely, a  
411 leaching experiment with de-ionized water showed a small increase in A<sub>T</sub> (Fig. 5) for both  
412 size fractions. By increasing the A<sub>T</sub> of freshwater, ash would act to increase the buffering  
413 capacity of river outflow into a typically weak carbonate system like the Reloncaví Fjord  
414 (Vergara-Jara et al., 2019). However, the absolute change in A<sub>T</sub> was relatively small despite  
415 the large ash loading used in all incubations (< 20 µmol kg<sup>-1</sup> A<sub>T</sub> for ash loading >4 g L<sup>-1</sup>) and  
416 therefore it is expected that the direct effect of ash on A<sub>T</sub> in situ was limited. Other effects on  
417 carbonate chemistry may however arise due to ash moderating the timing and intensity of  
418 primary production and thus biological pCO<sub>2</sub> drawdown.



419

420 Figure 5. Total alkalinity released after leaching 4.5 g L<sup>-1</sup> ash of two size fractions (<63 µm  
 421 and 250-1000 µm) in de-ionized water (DI water) and brackish water. T<sub>0</sub>= ‘time zero’,  
 422 measured after one minute of mixing, T<sub>2H</sub>= after two hours of mixing, T<sub>24H</sub>= after 24 hours  
 423 of mixing. n=4 for all treatments (mean ± standard deviation plotted). The initial (pre-ash  
 424 addition) alkalinity is marked by a black dot superimposed on the left T<sub>0</sub>. Source data is  
 425 provided in Supplementary Table 4.

426

427 Ion chromatography results for Na<sup>+</sup>, K<sup>+</sup>, Ca<sup>2+</sup>, F<sup>-</sup>, Cl<sup>-</sup>, NO<sub>3</sub><sup>-</sup> and SO<sub>4</sub><sup>2-</sup> showed that in the  
 428 presence of smaller ash size particles, ion inputs were generally higher (Table 2) as has been  
 429 reported previously (Jones and Gislason, 2008; Óskarsson, 1980; Rubin et al., 1994). The  
 430 leaching from ash components into de-ionized water occurred almost instantly with limited,  
 431 or no increases in leached concentrations observed between 0, 2 and 24 h (Table 2). For larger  
 432 particles there was less release of most ions. In the case of Ca<sup>2+</sup> and SO<sub>4</sub><sup>2-</sup> a more gradual

433 leaching effect was apparent (Table 2). The concentrations of  $\text{NO}_3^-$  and  $\text{NH}_4^+$  were generally  
 434 below detection suggesting that ash was a minor source of fixed-nitrogen into solution. These  
 435 observations are consistent with the trends in prior work using a range of volcanic ash and  
 436 incubation conditions (Duggen et al., 2010; Witham et al., 2005). Major ion analysis was  
 437 only conducted in de-ionized water as no significant changes would be observable for most  
 438 of these ions in brackish or saline waters under the same conditions.

439

440 Table 2. Major ion and macronutrient concentrations in  $\mu\text{mol/l}$  leached from the two size  
 441 fractions of ash ( $< 63 \mu\text{m}$  and  $250\text{-}1000 \mu\text{m}$ ) into deionized water (b.d. = below detection).  
 442 Shown are mean values, with the standard deviation in parentheses ( $n=4$ ). Also shown are  
 443 mass normalized values [ $\mu\text{mol/g}$  ash], and a comparison to the range of values reported by  
 444 Jones and Gislason (2008).

	Time [h]	$\text{Na}^+$	$\text{K}^+$	$\text{Ca}^{2+}$	$\text{F}^-$	$\text{Cl}^-$	$\text{SO}_4^{2-}$	$\text{NO}_3^-$	$\text{NH}_4^+$
<i>Detection limit</i>		0.17	0.43	0.30	0.28	1.31	1.64	0.34	0.13
<i>Proced. Blank</i>		b.d.	b.d.	0.39	b.d.	b.d.	b.d.	b.d.	b.d.
250-1000 $\mu\text{m}$	0.1	3.4 (2.8)	0.83 (0.3)	18.3 (3.3)	0.16 (0.05)	3.7 (1.9)	3.7 (2.2)	b.d.	0.15 (0.2)
[ $\mu\text{mol/l}$ ]	2	5.1 (2.0)	1.0 (0.2)	18.5 (4.5)	0.21 (0.08)	4.4 (1.6)	4.9 (2.0)	b.d.	0.38 (0.4)
	24	7.3 (0.1)	1.4 (0.2)	23.4 (3.2)	0.52 (0.18)	5.7 (0.5)	8.3 (2.1)	b.d.	b.d.
$<63 \mu\text{m}$	0.1	16.2 (12.7)	3.2 (0.3)	25.1 (5.4)	0.29 (0.0)	17.1 (13.6)	13.5 (1.3)	0.53 (0.2)	1.70 (1.1)
[ $\mu\text{mol/l}$ ]	2	16.7 (1.0)	3.8 (0.1)	31.8 (2.7)	0.63 (0.2)	15.2 (0.9)	19.0 (0.3)	b.d.	0.52 (1.0)
	24	17.3 (0.8)	3.9 (0.3)	33.8 (3.3)	0.69 (0.3)	14.6 (1.0)	18.8 (0.5)	b.d.	1.32 (2.6)
$<63 \mu\text{m}$	24	3.84	0.87	7.50	0.15	3.25	4.18	0.048	0.29
[ $\mu\text{mol/g}$ ash]	Range (lit.)	1.5-84.3	0.1-5.4	0.6-589	0.1-9	2-92.9	1-554	0-6.4	0.3-0.6

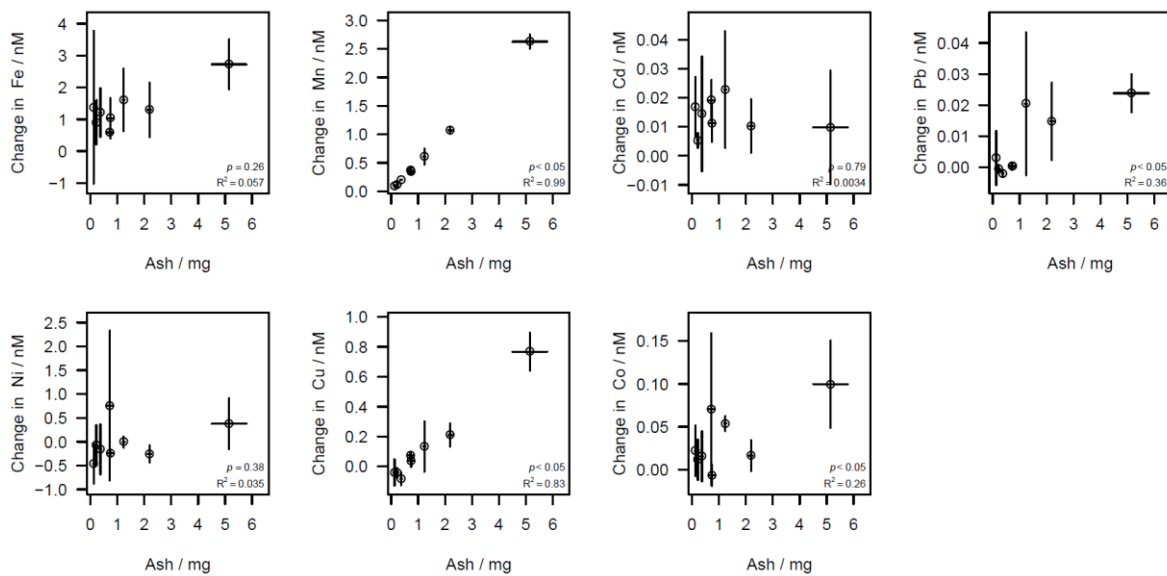
445

### 446 3.4 Trace elements in leach experiments

447 Release of nanomolar concentrations of dissolved Fe and Mn was evident when ash was re-  
 448 suspended in aged seawater for 10 minutes (Fig. 6). The net release of dissolved metals

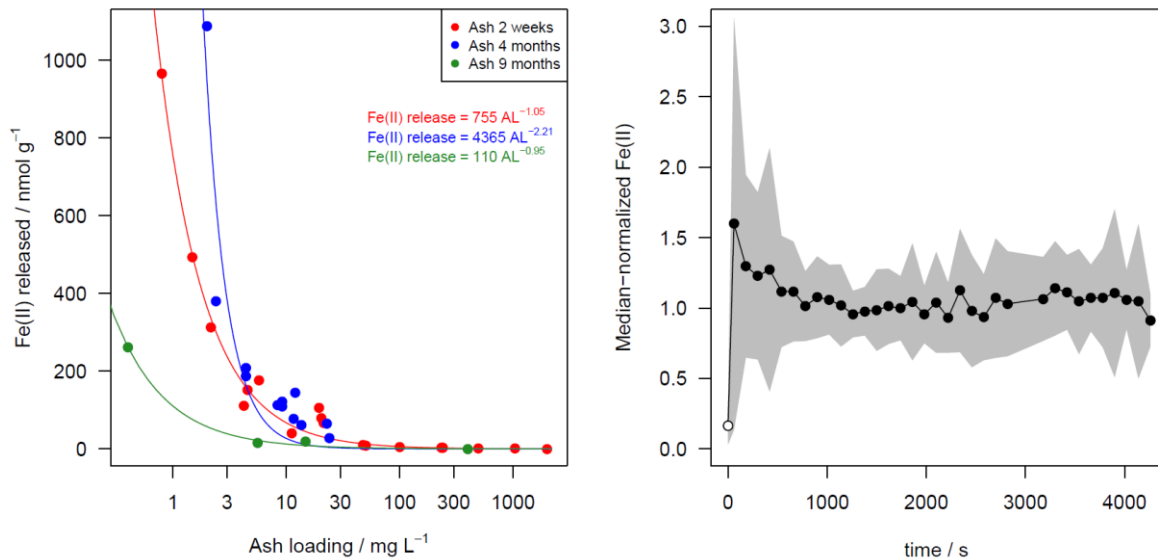
449 proceeded with varying relationships with ash loading over the applied gradient (2-50 mg L<sup>-1</sup>). Dissolved Mn, Pb, Cu and Co release exhibited significant ( $p < 0.05$ ) positive relationships  
450 with ash loading, with Mn and Cu exhibiting the most linear behavior ( $R^2$  0.99 and 0.83,  
451 respectively). Dissolved Fe, Cd and Ni showed no significant relationships with ash loading  
452 over the applied range. The initial concentration of metals in South Atlantic seawater should  
453 however also be considered when interpreting the trends. The magnitude of changes in Cd  
454 and Ni concentrations were smallest relative to both the initial concentration and the standard  
455 deviation on the initial concentration ( $0.38 \pm 0.04$  nM Cd and  $6.58 \pm 0.76$  nM Ni,  
456 respectively). It thus would be difficult to extract a clear relationship irrespective of their  
457 chemical behavior. For other elements (Fe, Co and Pb), non-linearity between ash addition  
458 and trace metal concentrations, and some negative changes in concentrations, both likely  
459 reflect scavenging of metal ions onto ash particle surfaces (Rogan et al., 2016). Fe, Co and  
460 Pb are all scavenged type elements and so increasing the surface area of ash present may  
461 affect the net change in metal concentration. The divergence between the behaviour of Mn  
462 and Fe, with Mn showing a stronger relationship with ash loading, supports the hypothesis  
463 of Mendez et al., (2010), that the release of dissolved Mn from aerosols into seawater depends  
464 primarily on ash Mn availability whereas the release of dissolved Fe is more dependent on  
465 the nature of organic material present in solution.  
466





467

468 Figure 6. Change in trace metal concentrations after varying ash addition to 100 ml South  
 469 Atlantic seawater for a 10-minute leach duration at room temperature. Initial (mean  $\pm$   
 470 standard deviation) dissolved trace metal concentrations - deducted from the final  
 471 concentrations to calculate the change as a result of ash addition - were  $0.98 \pm 0.03$  nM Fe,  
 472  $0.38 \pm 0.04$  nM Cd,  $13 \pm 2$  pM Pb,  $6.58 \pm 0.76$  nM Ni,  $0.84 \pm 0.07$  nM Cu,  $145 \pm 9$  pM Co,  
 473  $0.72 \pm 0.05$  nM Mn. Error bars are standard deviations from triplicate treatments with similar  
 474 ash loadings. p values and  $R^2$  for a linear regression are annotated. Source data is provided  
 475 in Supplementary Table 5. The same data with individual replicates is shown in  
 476 Supplementary Figure 1.



477

478 Figure 7. Fe(II) release from Calbuco ash into seawater. Mean Fe(II) released into South  
 479 Atlantic seawater over a 30 minute leach at 5-7°C (left). The same batch of Calbuco ash was  
 480 subsampled and used to conduct experiments on 3 occasions after the 2015 eruption (2 weeks,  
 481 4 months and 9 months since ash collection). The lines are power law fits, with associated  
 482 equations shown in the legend. The 3 time-series of Fe(II) concentrations following ash  
 483 addition is considered collectively by normalizing the measured concentrations (right), such  
 484 that 1.0 represents the median Fe(II) concentration measured in each experiment. All  
 485 experiments were conducted for at least 30 minutes, those conducted with 4/9 months old  
 486 ash were extended for 1 hour. The black line shows the mean response over 34 leach  
 487 experiments with varying ash loading, the shaded area shows  $\pm 1$  standard deviation. The  
 488 initial Fe(II) concentration (pre-ash addition at 0 s) in all cases was below detection and thus  
 489 the detection limit is plotted at 0 s (open circle). Source data is provided in Supplementary  
 490 Table 2.

491

492 In addition to the release of dFe in solution, which generally exists as Fe(III) species in oxic  
493 seawater (Gledhill and Buck, 2012), the release of Fe(II) was evident on a similar timescale  
494 when cold (5-7°C) aged S Atlantic seawater was used as leachate (Fig. 7). The half-life of  
495 Fe(II) decreases more than tenfold as temperature is increased from 5 to 25°C, leading to  
496 Fe(II) decay on timescales shorter than the time required for analysis (approximately 60 s for  
497 solution to enter the flow injection apparatus, mix with reagent and generate a peak)  
498 (Santana-Casiano et al., 2005). Elevated Fe(II) concentrations (mean 0.8 nM, Sup. Table 2)  
499 were evident at this temperature (5-7°C), which represents an intermediate sea surface  
500 temperature for the high latitude ocean. A sharp decline in Fe(II) dissolution efficiency with  
501 increasing ash load was also evident (Fig. 7). Both the highest Fe(II) concentration and the  
502 highest net release of Fe(II) were observed at the lowest ash loading (Fig. 7 and Sup. Fig. 2).  
503 Fe(II) concentration following dust addition into seawater was possibly reduced when the  
504 same experimental leaches with ash were repeated 9 months after the initial experiment. The  
505 first leaches were conducted ~2 weeks after ash collection. The absence of a clear change  
506 between 2 weeks and 4 months precludes an accurate assessment of the rate at which Fe(II)  
507 solubility may have decreased.

508

509 As Fe(II) concentrations were measured continuously using flow injection analysis, the  
510 temporal development of Fe(II) concentration after ash addition to cold seawater can also be  
511 shown (Fig. 7). Considering the set of leach experiments collectively, all ash additions were  
512 characterized by a sharp increase in Fe(II) concentrations in the first minute after ash addition  
513 into seawater. This was typically followed by a decline and then a relatively stable Fe(II)  
514 concentration (Fig. 7).

515 **3.5 Satellite observations**

516 Five-day composite images of atmospheric aerosol loading (UV aerosol index, which largely  
517 represents strongly UV-absorbing dust, Torres et al., 2007) indicated two main volcanic  
518 eruption plume trajectories following the major eruptions on 22 and 23 April: (i) northwards  
519 over the Pacific, and (ii) northeast over the Atlantic. Daily resolved time series were  
520 constructed for regions in the Atlantic and Pacific with elevated atmospheric aerosol loading  
521 (UV Aerosol Index  $\sim 2$  a.u.; Fig. 8). The Pacific time series indicated a pronounced peak in  
522 aerosol index followed by chlorophyll-a one day later. A control region to the south of the  
523 ash-impacted Pacific region showed no clear changes in chlorophyll-a matching that  
524 observed in the higher UV aerosol index region to the north (Sup. Fig. 3).

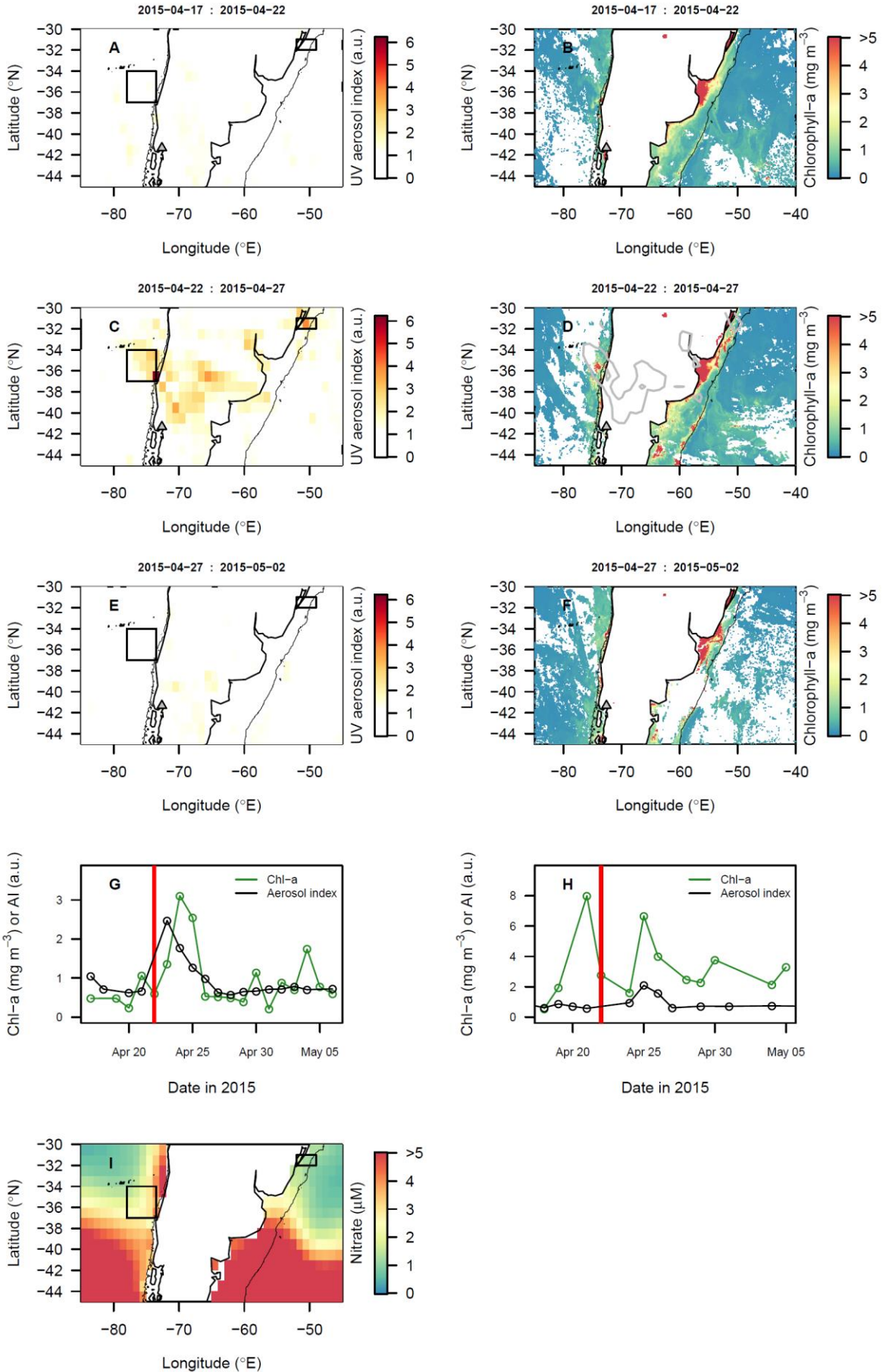
525

526 Conversely, in the Atlantic, where the background chlorophyll-a concentration was higher  
527 throughout the time period of interest, the main area with enhanced aerosol index was not  
528 clearly associated with a change in chlorophyll-a dynamics on a timescale comparable to that  
529 observed following other volcanic ash fertilized events (Fig. 8). In a smaller ash impacted  
530 area to the south of the Rio de la Plata (Sup. Fig. 3), where nitrate levels are expected to be  
531 higher than to the north and Fe levels also expected to be elevated due its location on the  
532 continental shelf, a chlorophyll-a peak was evident 7 days after the UV aerosol peak.  
533 However, this was not well constrained due to poor satellite coverage in the period after the  
534 eruption.

535

536 Prior eruptions have been attributed with driving time periods of enhanced regional marine  
537 primary production beginning 3-5 days post-eruption (Hamme et al., 2010; Langmann et al.,  
538 2010; Lin et al., 2011) and bottle experiments showing positive chlorophyll changes in

539 response to ash addition are typically significant compared to controls within 1-4 days  
540 following ash addition (Browning et al., 2014; Duggen et al., 2007; Mélançon et al., 2014).



542 Figure 8. Potential biological impact of the 2015 Calbuco eruption observed via satellite  
543 remote sensing. (A-F) Spatial maps showing the distribution of ash in the atmosphere (UV  
544 Aerosol Index) and corresponding images of chlorophyll-a. Images were composited over 5-  
545 day periods. Grey lines in chlorophyll maps corresponds to the UV Aerosol index = 2 a.u.  
546 contour. (G, H) Time series of UV Aerosol Index and chlorophyll-a for regions of the Pacific  
547 (G) and Atlantic (H) identified by boxes in maps. Red vertical lines (22 April) indicate the  
548 first eruption date. (I) Mean World Ocean Atlas surface NO<sub>3</sub> concentrations. Thin black lines  
549 indicate the 500 m bathymetric depth contour.

550

## 551 **4 Discussion**

### 552 **4.1 Local drivers of 2015 bloom dynamics in Reloncaví Fjord**

553 The north Patagonian archipelago and fjord region have a seasonal phytoplankton bloom  
554 cycle with peaks in productivity occurring in May and October (austral autumn and spring)  
555 and the lowest productivity consistently in June (austral winter)(González et al., 2010).  
556 Diatoms normally dominate the phytoplankton community during the productive period due  
557 to high light availability and high silicic acid supply, both of which are influenced by  
558 freshwater runoff (González et al., 2010; Torres et al., 2014). The austral fall season,  
559 encompassing the April-May 2015 ash deposition events, is therefore expected to have a high  
560 phytoplankton biomass (Iriarte et al., 2007; León-Muñoz et al., 2018) which terminates  
561 abruptly with decreasing light availability in austral winter (González et al., 2010).

562

563 Whilst not directly comparable, the magnitude of the 2015 bloom in terms of diatom  
564 abundance (Fig. 4) was more intense than that reported in Reloncaví Sound 2001-2008. With  
565 respect to the timing of the phytoplankton bloom, the low diatom abundances and

566 chlorophyll-a concentrations at the end of May (Fig. 4) are consistent with prior observations  
567 of sharp declines in primary production moving into June (González et al., 2010). Peaks in  
568 diatom abundance were measured at two stations on 14 May one week after the third (small)  
569 eruptive pulse, and measured chlorophyll-a concentrations were highest close to Station C  
570 on 30 April (Fig. 4). The high-resolution pH and O<sub>2</sub> data collected at Station C from mooring  
571 data is consistent with an intense phytoplankton bloom between ~29 April and 7 May (Fig.  
572 3) indicated by a shift to slightly higher pH and O<sub>2</sub> during this time period when river flow  
573 into the fjord was stable.

574

575 Without a direct measure of ash deposition per unit area in the fjord, turbidity, or higher  
576 resolution chlorophyll/diatom data, it is challenging to unambiguously determine the extent  
577 to which the austral autumn phytoplankton bloom was affected by volcanic activity. The high  
578 abundance of diatoms at two of three stations sampled could have resulted from ash  
579 fertilization. Yet if this was the case, it is not clear which nutrient was responsible for this  
580 fertilization, why the bloom initiation occurred about one week after the third eruptive pulse  
581 (several weeks after the main eruption events) and to what extent the timing was coincidental  
582 given that productivity normally peaks in May. Reloncaví Fjord was to the south of the  
583 dominant ash deposition from the 22 and 23 April eruptions (Romero et al., 2016) and thus  
584 ash was delivered by a mixture of vectors including runoff and rainfall. The Petrohue river  
585 basin was particularly severely affected by ash with deposition of up to 50 cm ash in places.  
586 This complicates the interpretation of the time series provided by high resolution data (Fig.  
587 3). With incident light also highly variable over the time series (Fig. 3F), there are clearly  
588 several factors, other than volcanic ash deposition, which will have exerted some influence  
589 on diatom and chlorophyll-a abundance throughout May 2015.



590

591 Primary production in the Reloncaví region is thought to be limited by light availability rather  
592 than macronutrient availability (González et al., 2010). Whilst micronutrient availability  
593 relative to phytoplankton demand has not been extensively assessed in this fjord, with such  
594 higher riverine inputs across the region- which are normally a large source of dissolved trace  
595 elements into coastal waters (e.g. Boyle et al., 1977)- limitation of phytoplankton growth by  
596 Fe, or another micronutrient, seems implausible. Reported Fe concentrations determined by  
597 a diffusive gel technique in Reloncaví Fjord in October 2006 were relatively high; 46-530  
598 nM (Ahumada et al., 2011). Similarly, reported dFe concentrations in the adjacent Comau  
599 Fjord at higher salinity are generally in the nanomolar range and remain >2 nM even under  
600 post-bloom conditions which suggests dFe is not a limiting factor for phytoplankton growth  
601 (Hopwood et al., 2020; Sanchez et al., 2019).

602

603 Silicic acid availability could have been increased by ash deposition. Whilst not quantified  
604 herein, an increase in silicic acid availability from ash in a region where silicic acid was sub-  
605 optimal for diatom growth could plausibly explain higher than usual diatom abundance  
606 (Siringan et al., 2018). Silicic acid concentrations were indeed high (up to 118  $\mu\text{M}$ ) in  
607 Reloncaví Fjord surface waters and >30  $\mu\text{M}$  at 15 m depth (salinity 33.4) (Vergara-Jara et  
608 al., 2019; Yevenes et al., 2019). However concentrations >30  $\mu\text{M}$  are typical during periods  
609 of high runoff and accordingly are not thought to limit primary production or diatom growth  
610 in this area (González et al., 2010). The  $\text{Si}(\text{OH})_4:\text{NO}_3$  ratio in Reloncaví Fjord and  
611 downstream Reloncaví Sound also indicates an excess of  $\text{Si}(\text{OH})_4$ , with ratios of  
612 approximately 2:1 observed in fjord surface waters throughout the year (González et al.,  
613 2010; Yevenes et al., 2019). For comparison, the ratio of Si:N for diatom nutrient uptake is

614 15:16 (Brzezinski, 1985). Furthermore, experimental incubations making additions of  
615 macronutrients to fjord waters in Reloncaví and adjacent fjords, have found strong responses  
616 of phytoplankton to additions of silicic acid only when  $\text{Si(OH)}_4$  and  $\text{NO}_3$  were added in  
617 combination, further corroborating the hypothesis that an excess of silicic acid is normally  
618 present in surface waters of these fjord systems (Labbé-Ibáñez et al., 2015). It is therefore  
619 doubtful that changes in nutrient availability from ash alone could explain such high diatom  
620 abundances in mid-May.

621

622 Alternative reasons for high diatom abundances in the absence of a chemical fertilization  
623 effect are plausible and could include, for example, ash having reduced zooplankton  
624 abundance or virus activity in the fjord, thus facilitating higher diatom abundance than would  
625 otherwise have been observed by decreasing diatom mortality rates in an environment where  
626 nutrients were replete. The role of volcanic ash in driving such short-term ecological shifts  
627 in the marine environment is almost entirely unstudied (Weinbauer et al., 2017). However,  
628 volcanic ash deposition of  $7 \text{ mg L}^{-1}$  in lakes within this region during the 2011 Puyehue-  
629 Cordón Caulle eruption was reported to increase post-deposition phytoplankton biomass and  
630 decrease copepod and cladoceran biomass (Wolinski et al., 2013). The proposed mechanism  
631 was ash particle ingestion negatively affecting zooplankton, and ash-shading positively  
632 affecting phytoplankton via reduced photoinhibition (Balseiro et al., 2014; Wolinski et al.,  
633 2013).

634

635 Considering the more modest peak in diatom abundance at the most strongly ash affected  
636 station (Station A, Fig. 4) and the timing of the peak diatom abundance 3 weeks after the  
637 main eruption, it is clear that the interaction between ash and phytoplankton in the Reloncaví

638 Fjord was more complex than the simple Fe-fertilization proposed for the SE Pacific (Fig.  
639 8g). In the absence of an immediate diatom fertilization effect from Fe or silicic acid, we  
640 hypothesize that any change in phytoplankton bloom dynamics within Reloncaví Fjord was  
641 mainly a ‘top-down’ effect driven by the physical interaction of ash and different ecological  
642 groups in a nutrient replete environment, rather than a ‘bottom-up’ effect driven by  
643 alleviation of nutrient-limitation from ash dissolution.

#### 644 **4.2 Volcanic ash as a unique source of trace elements**

645 The release of the bioessential elements Fe and Mn from ash here ranged from 53 - 1200  
646  $\text{nmol g}^{-1}$  (dFe) and 48 - 71  $\text{nmol g}^{-1}$  (dissolved Mn). For dFe this is comparable to the rates  
647 determined in other studies under similar experimental conditions for subduction zone  
648 volcanic ash, with reported Fe-release in prior work ranging 2-570  $\text{nmol g}^{-1}$  (Sup. Table 1).  
649 For Mn, less prior work is available, but these values are within the 17-1300  $\text{nmol g}^{-1}$  range  
650 reported by Hoffmann et al., (2012). Fe(II) release was particularly efficient at ash loadings  
651  $<5 \text{ mg L}^{-1}$  (Fig. 7), whereas dFe release was less sensitive to ash loading (Fig. 6). The timing  
652 of Fe(II) release in the first 60 s of incubations suggests a fast dissolution process. Fe(II) is  
653 short lived in oxic surface seawater with an observed half-life of only 10-20 minutes even in  
654 the Southern Ocean where cold surface waters slow Fe(II) oxidation (Sarhou et al., 2011).  
655 Yet, relative to Fe(III), Fe(II) is also more soluble and, from an energetic perspective,  
656 expected to be more bioaccessible to cellular uptake (Sunda et al., 2001). Whilst it is known  
657 that the vast majority of dFe leached from ash into seawater tends to occur in the first minutes  
658 of ash addition (Duggen et al., 2007; Jones and Gislason, 2008), and this could be consistent  
659 with rapid dissolution of highly soluble phases on ash surfaces, we note that there is not yet  
660 conclusive evidence concerning the precise origin of this dFe pulse. Fe(II) salts may be  
661 present on the surface of ash particles (Horwell et al., 2003; Hoshyaripour et al., 2015) and

662 thus the Fe(II) observed herein (Fig. 7) may reflect almost instantaneous release following  
663 dissolution of thin layers of salt coatings in ash surfaces (Ayriss and Delmelle, 2012; Delmelle  
664 et al., 2007; Olsson et al., 2013). Alternatively Fe(II) could be released from more crystalline  
665 Fe(II) phases. Prior work, at much lower pH (pH 1 H<sub>2</sub>SO<sub>4</sub> representing conditions that ash  
666 surfaces may experience during atmospheric processing, but not in aquatic environments)  
667 suggests that short-term release of Fe(II) or Fe(III) is determined by the surface Fe(II)/Fe  
668 ratio which may differ from the bulk Fe(II)/Fe ratio due to plume processing (Maters et al.,  
669 2017).

670 Different leaching protocols are widely recognised as a major challenge for interpreting and  
671 comparing different dissolution experiment datasets for all types of aerosols (Duggen et al.,  
672 2007; Morton et al., 2013). When Fe(II) is released into solution as a considerable fraction  
673 of the total dFe release this is particularly challenging to monitor, as Fe(II) oxidises on  
674 timescales of seconds to minutes depending on temperature, pH and O<sub>2</sub> conditions (Santana-  
675 Casiano et al., 2005). The dFe and Fe(II) leaching protocols used herein are only comparable  
676 qualitatively, as the Fe(II) method using cooler seawater and larger seawater volumes was  
677 specifically designed to test for the presence of rapid Fe(II) release and to evaluate the short-  
678 term temporal trend of any such release. Yet, for rough comparative purposes, the Fe(II)  
679 released was equivalent to  $38 \pm 25\%$  (mean  $\pm$  standard deviation) of dFe released at ash  
680 loadings from 1-10 mg L<sup>-1</sup> and  $19 \pm 17\%$  of dFe for ash loadings from 10-50 mg L<sup>-1</sup>. These  
681 values are reasonably comparable to the 26% median Fe(II)/dFe fraction measured in Fe  
682 released into seawater from aerosols collected across zonal transects of the Pacific Ocean  
683 (Buck et al., 2013) suggesting that fresh Calbuco ash is roughly comparable in terms of Fe(II)  
684 lability to these environmentally processed aerosols.

#### 685 **4.3 A potential fertilization effect in the SE Pacific**

686 Experiments with ash suspensions have shown that ash loading has a restricted impact on  
687 satellite chlorophyll-a retrieval (Browning et al., 2015), therefore offering a means to assess  
688 the potential biological impact of the 2015 Calbuco eruption in offshore waters. We found  
689 evidence for fertilization of offshore Pacific seawaters in the studied area (Fig. 8). Following  
690 the eruption date, mean chlorophyll-a concentrations increased ~2.5 times over a broad  
691 region where elevated UV aerosol index was detected (Fig. 8G). Both the timing and location  
692 of this chlorophyll-a peak were consistent with ash fertilization, with the peak of elevated  
693 chlorophyll-a being located within the core of highest atmospheric aerosol loading, and the  
694 peak date occurring one day after the main passage of the atmospheric aerosol plume. A  
695 similar phytoplankton response timeframe was reported following ash deposition in the NE  
696 Pacific following the August 2008 Kasatochi eruption (Hamme et al., 2010) which was  
697 similarly thought to be triggered by relief of Fe-limitation (Langmann et al., 2010). At the  
698 same time, a control region to the south of the ash-impacted Pacific region showed no clear  
699 changes in chlorophyll-a matching that observed in the higher UV aerosol index region to  
700 the north (Sup. Fig. 3).

701

702 In the SW Atlantic, two ash impacted areas are highlighted; one to the north (Fig. 8), and one  
703 to the south of the Rio de la Plata (Sup. Fig. 3). Nitrate levels are expected to be higher in the  
704 south than to the north, with Fe levels expected to be elevated across both locations as a result  
705 of their position on the continental shelf. In the area to the north of the Rio de la Plata (Fig.  
706 8), ash deposition indicated by the UV aerosol index did not lead to such a clear  
707 corresponding change in chlorophyll-a concentrations (Fig. 8H), although with the available  
708 data it is not possible to rule out the possibility of fertilisation completely (e.g., whilst also  
709 being preceded by a larger chlorophyll-a peak on 21 April, there is a peak in chlorophyll-a

710 at 25 April coinciding with elevated UV aerosol index). Phytoplankton growth in this region  
711 of the Atlantic is expected to be limited by fixed nitrogen availability, as a result of strong  
712 stratification (Moore et al., 2013) and thus dFe release from ash particles alone would not be  
713 expected to result in short-term increases to primary production. In the second area of ash  
714 deposition, to the south (Sup. Fig. 3), a chlorophyll-a peak was evident 7 days after the UV  
715 aerosol peak. However, this was not well constrained due to poor satellite coverage in the  
716 period after the eruption. Considering the dynamic spatial and temporal variation in  
717 chlorophyll within this coastal area, it is challenging to associate any change in chlorophyll  
718 specifically with ash arrival.

719

720 The change in chlorophyll-a observed in the SE Pacific contrasts with results in Reloncaví  
721 Fjord where phytoplankton abundances likely peaked much later than the first ash arrival-  
722 after 28 April. The fertilized region of the Pacific (Fig. 8) hosts upwelling of deep waters,  
723 supplying nutrients in ratios that are deficient in dFe (Bonnet et al., 2008; Torres and  
724 Ampuero, 2009). Fe-limitation of phytoplankton growth in this region is therefore  
725 anticipated, which could have been temporarily relieved following ash deposition and dFe  
726 release (Fig. 6). The differential responses observed in the Pacific and Atlantic are therefore  
727 consistent with the anticipated nutrient limitation regimes (Fe-limited and nitrogen-limited,  
728 respectively), and the supply of dFe but not fixed N ( $\text{NO}_3$  or  $\text{NH}_4$ ) from the Calbuco ash (Fig.  
729 6 and Table 2).

730

## 731 **5 Conclusions**

732 The contrasting effects of volcanic ash on primary producers in Reloncaví Fjord, the SE  
733 Pacific and SW Atlantic Oceans support the hypothesis that the response of primary

734 producers is dependent on both the ash loading and the resources limiting primary production  
735 in a region at a specific time of year. Leach experiments using ash from the 2015 Calbuco  
736 eruption demonstrated a small increase in the alkalinity of de-ionized water from fine, but  
737 not coarse ash, and no significant addition of fixed nitrogen (quantified as  $\text{NO}_3$  and  $\text{NH}_4$ ) into  
738 solution. In saline waters, release of dissolved trace metals including Mn, Cu, Co, Pb, Fe and  
739 specifically Fe(II) was evident.

740

741 Strong evidence of a broad-scale ‘bottom-up’ fertilization effect of ash on phytoplankton was  
742 not found locally within Reloncaví Fjord, although it is possible that the timing and peak  
743 diatom abundance of the autumn phytoplankton bloom may have shifted in response to high  
744 ash loading in the weeks following the first eruption. High diatom abundances at some  
745 stations within the fjord several weeks after the eruption may have arisen from a ‘top-down’  
746 effect of ash on filter feeders, although the mechanism can only be speculated herein. No  
747 clear positive effect of ash deposition on chlorophyll-a was evident in the SW Atlantic,  
748 consistent with expected patterns in nutrient deficiency which suggest the region to be  
749 nitrogen-limited. However, in offshore waters of the SE Pacific where Fe is anticipated to  
750 limit phytoplankton growth, a chlorophyll-a increase was related with maximum ash  
751 deposition and we presume that this increase in chlorophyll-a was likely driven by Fe-  
752 fertilization.

753

## 754 **6. Data availability**

755 The complete 2015 time series from the Reloncaví Fjord mooring is available online  
756 ([https://figshare.com/articles/Puelo\\_Bouy/7754258](https://figshare.com/articles/Puelo_Bouy/7754258)). Source data for Figures 4-7 is included  
757 in the Supplement.

758

## 759 **7. Acknowledgements**

760 The authors thank the Dirección de Investigación & Desarrollo UACH for its partial support  
761 during this project. The data presented are part of the second chapter of the PhD Thesis of  
762 MVJ at Universidad Austral de Chile. Cristian Vargas (Universidad de Concepción) is  
763 thanked for making additional chlorophyll a data available, Manuel Díaz for providing Fig.  
764 1, Lorena Rebolledo for running the particle size test, Miriam Beck for assistance with Fe(II)  
765 flow injection analysis and 3 reviewers for constructive comments that improved the  
766 manuscript.

767

## 768 **8. Funding**

769 JLI and EA gratefully acknowledge funding from the European Commission (OCEAN-  
770 CERTAIN, FP7- ENV- 2013-6.1-1; no: 603773). JLI received funding by CONICYT-  
771 FONDECYT 1141065 and is partially funded by Center IDEAL (FONDAP 15150003).  
772 Partial funding came from CONICYT-FONDECYT 1140385 (RT). MVJ received financial  
773 support from a CONICYT Scholarship (Beca Doctorado Nacional 2015 No 21150285). IR  
774 and MH received funding from the Deutsche Forschungsgemeinschaft as part of  
775 Sonderforschungsbereich (SFB) 754: 'Climate-Biogeochemistry Interactions in the Tropical  
776 Ocean'.

777

## 778 **9. Author contributions**

779 MVJ, MH, JLI and EA designed the study. MVJ, IR, MH, RT and BR conducted analytical  
780 and field work. TB conducted satellite data analysis. MV, MH and TB wrote the initial  
781 manuscript with all authors contributing to its revision.



782

783 **10. References**

784 Achterberg, E. ., Moore, C. M., Henson, S. A., Steigenberger, S., Stohl, A., Eckhardt, S.,

785 Avendano, L. C., Cassidy, M., Hembury, D., Klar, J. K., Lucas, M. I., MacEy, A. I.,

786 Marsay, C. M. and Ryan-Keogh, T. J.: Natural iron fertilization by the Eyjafjallajokull

787 volcanic eruption, *Geophys. Res. Lett.*, 40(5), 921–926, doi:10.1002/grl.50221, 2013.

788 Ahumada, R., Rudolph, A., Gonzalez, E., Fones, G., Saldias, G. and Ahumada Rudolph, R.:

789 Dissolved trace metals in the water column of Reloncavi Fjord, Chile, *Lat. Am. J. Aquat.*

790 *Res.*, 39, 567–574, doi:10.3856/vol39-issue3-fulltext-16, 2011.

791 Ayris, P. and Delmelle, P.: Volcanic and atmospheric controls on ash iron solubility: A

792 review, *Phys. Chem. Earth*, doi:10.1016/j.pce.2011.04.013, 2012.

793 Baker, A. R. and Croot, P. L.: Atmospheric and marine controls on aerosol iron solubility

794 in seawater, *Mar. Chem.*, 120(1–4), 4–13, doi:10.1016/j.marchem.2008.09.003, 2010.

795 Balseiro, E., Souza, M. S., Olabuenaga, I. S., Wolinski, L., Navarro, M. B.,

796 Laspoumaderes, C. and Modenutti, B.: Effect of the Puyehue-Cordon Caulle volcanic

797 complex eruption on crustacean zooplankton of Andean Lakes, *Ecol. Austral*, 24, 75–82,

798 2014.

799 Bonnet, S., Guieu, C., Bruyant, F., Prášil, O., Van Wambeke, F., Raimbault, P., Moutin, T.,

800 Grob, C., Gorbunov, M. Y., Zehr, J. P., Masquelier, S. M., Garczarek, L. and Claustre, H.:

801 Nutrient limitation of primary productivity in the Southeast Pacific (BIOSOPE cruise),

802 *Biogeosciences*, 5(1), 215–225, doi:10.5194/bg-5-215-2008, 2008.

803 Boyle, E. A., Edmond, J. M. and Sholkovitz, E. R.: Mechanism of iron removal in

804 estuaries, *Geochim. Cosmochim. Acta*, 41(9), 1313–1324, doi:10.1016/0016-

805 7037(77)90075-8, 1977.

806 Browning, T. J., Bouman, H. A., Henderson, G. M., Mather, T. A., Pyle, D. M., Schlosser,  
807 C., Woodward, E. M. S. and Moore, C. M.: Strong responses of Southern Ocean  
808 phytoplankton communities to volcanic ash, *Geophys. Res. Lett.*, 41(8), 2851–2857,  
809 doi:10.1002/2014GL059364, 2014.

810 Browning, T. J., Stone, K., Bouman, H., Mather, T. A., Pyle, D. M., Moore, M. and  
811 Martinez-Vicente, V.: Volcanic ash supply to the surface ocean – remote sensing of  
812 biological responses and their wider biogeochemical significance, *Front. Mar. Sci.*, 2,  
813 doi:10.3389/fmars.2015.00014, 2015.

814 Brzezinski, M. A.: The Si:C:N ratio of marine diatoms: interspecific variability and the  
815 effect of some environmental variables, *J. Phycol.*, 21(3), 347–357, doi:10.1111/j.0022-  
816 3646.1985.00347.x, 1985.

817 Buck, C. S., Landing, W. M. and Resing, J.: Pacific Ocean aerosols: Deposition and  
818 solubility of iron, aluminum, and other trace elements, *Mar. Chem.*, 157, 117–130,  
819 doi:10.1016/j.marchem.2013.09.005, 2013.

820 Cáceres, M., Valle-Levinson, A., Sepúlveda, H. H. and Holderied, K.: Transverse  
821 variability of flow and density in a Chilean fjord, in *Continental Shelf Research.*, 2002.

822 Castillo, M. I., Cifuentes, U., Pizarro, O., Djurfeldt, L. and Cáceres, M.: Seasonal  
823 hydrography and surface outflow in a fjord with a deep sill: The Reloncaví fjord, Chile,  
824 *Ocean Sci.*, 12, 533–544, doi:10.5194/os-12-533-2016, 2016.

825 DeGrandpre, M. D., Hammar, T. R., Smith, S. P. and Sayles, F. L.: In situ measurements of  
826 seawater pCO<sub>2</sub>, *Limnol. Oceanogr.*, 40(5), 969–975, doi:10.4319/lo.1995.40.5.0969, 1995.

827 DeGrandpre, M. D., Baehr, M. M. and Hammar, T. R.: Calibration-free optical chemical  
828 sensors, *Anal. Chem.*, 71(6), 1152–1159, doi:10.1021/ac9805955, 1999.

829 Delmelle, P., Lambert, M., Dufrière, Y., Gerin, P. and Óskarsson, N.: Gas/aerosol-ash

830 interaction in volcanic plumes: New insights from surface analyses of fine ash particles,  
831 Earth Planet. Sci. Lett., 259, 159–170, doi:10.1016/j.epsl.2007.04.052, 2007.

832 Duggen, S., Croot, P., Schacht, U. and Hoffmann, L.: Subduction zone volcanic ash can  
833 fertilize the surface ocean and stimulate phytoplankton growth: Evidence from  
834 biogeochemical experiments and satellite data, Geophys. Res. Lett.,  
835 doi:10.1029/2006GL027522, 2007.

836 Duggen, S., Olgun, N., Croot, P., Hoffmann, L., Dietze, H., Delmelle, P. and Teschner, C.:  
837 The role of airborne volcanic ash for the surface ocean biogeochemical iron-cycle: a  
838 review, Biogeosciences, 7(3), 827–844, doi:10.5194/bg-7-827-2010, 2010.

839 Van Eaton, A. R., Amigo, Á., Bertin, D., Mastin, L. G., Giacosa, R. E., González, J.,  
840 Valderrama, O., Fontijn, K. and Behnke, S. A.: Volcanic lightning and plume behavior  
841 reveal evolving hazards during the April 2015 eruption of Calbuco volcano, Chile,  
842 Geophys. Res. Lett., 43(7), 3563–3571, doi:10.1002/2016GL068076, 2016.

843 Ermolin, M. S., Fedotov, P. S., Malik, N. A. and Karandashev, V. K.: Nanoparticles of  
844 volcanic ash as a carrier for toxic elements on the global scale, Chemosphere, 200, 16–22,  
845 doi:10.1016/j.chemosphere.2018.02.089, 2018.

846 Frogner, P., Gislason, S. R. and Oskarsson, N.: Fertilizing potential of volcanic ash in  
847 ocean surface water, Geology, 29(6), 487–490, doi:10.1130/0091-  
848 7613(2001)029<0487:fpovai>2.0.co;2, 2001.

849 Gledhill, M. and Buck, K. N.: The organic complexation of iron in the marine environment:  
850 a review, Front. Microbiol., 3, 69, doi:10.3389/fmicb.2012.00069, 2012.

851 González, H. E., Calderón, M. J., Castro, L., Clement, A., Cuevas, L. A., Daneri, G., Iriarte,  
852 J. L., Lizárraga, L., Martínez, R., Menschel, E., Silva, N., Carrasco, C., Valenzuela, C.,  
853 Vargas, C. A. and Molinet, C.: Primary production and plankton dynamics in the Reloncaví

854 Fjord and the Interior Sea of Chiloé, Northern Patagonia, Chile, *Mar. Ecol. Prog. Ser.*, 402,  
855 13–30, 2010.

856 Hamme, R. C., Webley, P. W., Crawford, W. R., Whitney, F. A., Degrandpre, M. D.,  
857 Emerson, S. R., Eriksen, C. C., Giesbrecht, K. E., Gower, J. F. R., Kavanaugh, M. T., Pea,  
858 M. A., Sabine, C. L., Batten, S. D., Coogan, L. A., Grundle, D. S. and Lockwood, D.:  
859 Volcanic ash fuels anomalous plankton bloom in subarctic northeast Pacific, *Geophys. Res.*  
860 *Lett.*, 37(19), L19604, doi:10.1029/2010GL044629, 2010.

861 Haraldsson, C., Anderson, L. G., Hassellöv, M., Hulth, S. and Olsson, K.: Rapid, high-  
862 precision potentiometric titration of alkalinity in ocean and sediment pore waters, *Deep Sea*  
863 *Res. Part I Oceanogr. Res. Pap.*, 44(12), 2031–2044, doi:10.1016/S0967-0637(97)00088-5,  
864 1997.

865 Hasle, G. R.: The inverted-microscope method, in *Phytoplankton manual.*, 1978.

866 Hoffmann, L. J., Breitbarth, E., Ardelan, M. V., Duggen, S., Olgun, N., Hassellöv, M. and  
867 Wängberg, S.-Å.: Influence of trace metal release from volcanic ash on growth of  
868 *Thalassiosira pseudonana* and *Emiliana huxleyi*, *Mar. Chem.*, 132–133, 28–33,  
869 doi:10.1016/j.marchem.2012.02.003, 2012.

870 Hopwood, M. J., Santana-González, C., Gallego-Urrea, J., Sanchez, N., Achterberg, E. P.,  
871 Ardelan, M. V., Gledhill, M., González-Dávila, M., Hoffmann, L., Leiknes, Ø., Magdalena  
872 Santana-Casiano, J., Tsagaraki, T. M. and Turner, D.: Fe(II) stability in coastal seawater  
873 during experiments in Patagonia, Svalbard, and Gran Canaria, *Biogeosciences*,  
874 doi:10.5194/bg-17-1327-2020, 2020.

875 Horwell, C. J., Fenoglio, I., Vala Ragnarsdottir, K., Sparks, R. S. J. and Fubini, B.: Surface  
876 reactivity of volcanic ash from the eruption of Soufrière Hills volcano, Montserrat, West  
877 Indies with implications for health hazards, *Environ. Res.*, 93(2), 202–215,

878 doi:10.1016/S0013-9351(03)00044-6, 2003.

879 Hoshyaripour, G. A., Hort, M. and Langmann, B.: Ash iron mobilization through  
880 physicochemical processing in volcanic eruption plumes: A numerical modeling approach,  
881 *Atmos. Chem. Phys.*, 15, 9361–9379, doi:10.5194/acp-15-9361-2015, 2015.

882 Hu, C., Lee, Z. and Franz, B.: Chlorophyll algorithms for oligotrophic oceans: A novel  
883 approach based on three-band reflectance difference, *J. Geophys. Res. Ocean.*, 117(C1),  
884 doi:10.1029/2011JC007395, 2012.

885 Iriarte, J. L., González, H. E., Liu, K. K., Rivas, C. and Valenzuela, C.: Spatial and  
886 temporal variability of chlorophyll and primary productivity in surface waters of southern  
887 Chile (41.5–43° S), *Estuar. Coast. Shelf Sci.*, 74(3), 471–480,  
888 doi:10.1016/j.ecss.2007.05.015, 2007.

889 Jones, M. R., Nightingale, P. D., Turner, S. M. and Liss, P. S.: Adaptation of a load-inject  
890 valve for a flow injection chemiluminescence system enabling dual-reagent injection  
891 enhances understanding of environmental Fenton chemistry, *Anal. Chim. Acta*, 796, 55–60,  
892 doi:10.1016/j.aca.2013.08.003, 2013.

893 Jones, M. T. and Gislason, S. R.: Rapid releases of metal salts and nutrients following the  
894 deposition of volcanic ash into aqueous environments, *Geochim. Cosmochim. Acta*, 72(15),  
895 3661–3680, doi:10.1016/j.gca.2008.05.030, 2008.

896 Labbé-Ibáñez, P., Iriarte, J. L. and Pantoja, S.: Respuesta del microfitoplancton a la adición  
897 de nitrato y ácido silícico en fiordos de la Patagonia chilena, *Lat. Am. J. Aquat. Res.*, 43(1),  
898 80–93, doi:10.3856/vol43-issue1-fulltext-8, 2015.

899 Langmann, B., Zakšek, K., Hort, M. and Duggen, S.: Volcanic ash as fertiliser for the  
900 surface ocean, *Atmos. Chem. Phys.*, 10, 3891–3899, doi:10.5194/acp-10-3891-2010, 2010.

901 León-Muñoz, J., Marcé, R. and Iriarte, J. L.: Influence of hydrological regime of an Andean

902 river on salinity, temperature and oxygen in a Patagonia fjord, Chile, *New Zeal. J. Mar.*  
903 *Freshw. Res.*, 47(4), 515–528, doi:10.1080/00288330.2013.802700, 2013.

904 León-Muñoz, J., Urbina, M. A., Garreaud, R. and Iriarte, J. L.: Hydroclimatic conditions  
905 trigger record harmful algal bloom in western Patagonia (summer 2016), *Sci. Rep.*, 8(1),  
906 1330, doi:10.1038/s41598-018-19461-4, 2018.

907 Lin, I. I., Hu, C., Li, Y. H., Ho, T. Y., Fischer, T. P., Wong, G. T. F., Wu, J., Huang, C. W.,  
908 Chu, D. A., Ko, D. S. and Chen, J. P.: Fertilization potential of volcanic dust in the low-  
909 nutrient low-chlorophyll western North Pacific subtropical gyre: Satellite evidence and  
910 laboratory study, *Global Biogeochem. Cycles*, 25, GB1006, doi:10.1029/2009GB003758,  
911 2011.

912 López-Escobar, L., Parada, M. A., Hickey-Vargas, R., Frey, F. A., Kempton, P. D. and  
913 Moreno, H.: Calbuco Volcano and minor eruptive centers distributed along the Liquiñe-  
914 Ofqui Fault Zone, Chile (41°–42° S): contrasting origin of andesitic and basaltic magma in  
915 the Southern Volcanic Zone of the Andes, *Contrib. to Mineral. Petrol.*, 119(4), 345–361,  
916 doi:10.1007/BF00286934, 1995.

917 Martin, J. H., Fitzwater, S. E. and Gordon, R. M.: Iron deficiency limits phytoplankton  
918 growth in Antarctic waters, *Global Biogeochem. Cycles*, 4(1), 5–12, 1990.

919 Maters, E. C., Delmelle, P. and Gunnlaugsson, H. P.: Controls on iron mobilisation from  
920 volcanic ash at low pH: Insights from dissolution experiments and Mössbauer  
921 spectroscopy, *Chem. Geol.*, 449, 73–81, doi:10.1016/j.chemgeo.2016.11.036, 2017.

922 Mélançon, J., Levasseur, M., Lizotte, M., Delmelle, P., Cullen, J., Hamme, R. C., Peña, A.,  
923 Simpson, K. G., Scarratt, M., Tremblay, J. É., Zhou, J., Johnson, K., Sutherland, N.,  
924 Arychuk, M., Nemcek, N. and Robert, M.: Early response of the northeast subarctic Pacific  
925 plankton assemblage to volcanic ash fertilization, *Limnol. Oceanogr.*, 59,

926 doi:10.4319/lo.2014.59.1.0055, 2014.

927 Mendez, J., Guieu, C. and Adkins, J.: Atmospheric input of manganese and iron to the  
928 ocean: Seawater dissolution experiments with Saharan and North American dusts, *Mar.*  
929 *Chem.*, 120(1), 34–43, doi:10.1016/j.marchem.2008.08.006, 2010.

930 Millero, F. J., Sotolongo, S. and Izaguirre, M.: The oxidation-kinetics of Fe(II) in seawater,  
931 *Geochim. Cosmochim. Acta*, 51(4), 793–801, doi:10.1016/0016-7037(87)90093-7, 1987.

932 Molinet, C., Díaz, M., Marín, S. L., Astorga, M. P., Ojeda, M., Cares, L. and Asencio, E.:  
933 Relation of mussel spatfall on natural and artificial substrates: Analysis of ecological  
934 implications ensuring long-term success and sustainability for mussel farming,  
935 *Aquaculture*, 467, 211–218, doi:10.1016/j.aquaculture.2016.09.019, 2017.

936 Moore, C. M., Mills, M. M., Arrigo, K. R., Berman-Frank, I., Bopp, L., Boyd, P. W.,  
937 Galbraith, E. D., Geider, R. J., Guieu, C., Jaccard, S. L., Jickells, T. D., La Roche, J.,  
938 Lenton, T. M., Mahowald, N. M., Marañón, E., Marinov, I., Moore, J. K., Nakatsuka, T.,  
939 Oschlies, A., Saito, M. A., Thingstad, T. F., Tsuda, A. and Ulloa, O.: Processes and  
940 patterns of oceanic nutrient limitation, *Nat. Geosci.*, doi:10.1038/ngeo1765, 2013.

941 Morton, P. L., Landing, W. M., Hsu, S. C., Milne, A., Aguilar-Islas, A. M., Baker, A. R.,  
942 Bowie, A. R., Buck, C. S., Gao, Y., Gichuki, S., Hastings, M. G., Hatta, M., Johansen, A.  
943 M., Losno, R., Mead, C., Patey, M. D., Swarr, G., Vandermark, A. and Zamora, L. M.:  
944 Methods for the sampling and analysis of marine aerosols: Results from the 2008  
945 GEOTRACES aerosol intercalibration experiment, *Limnol. Oceanogr. Methods*, 11,  
946 doi:10.4319/lom.2013.11.62, 2013.

947 Mosley, L. M., Husheer, S. L. G. and Hunter, K. A.: Spectrophotometric pH measurement  
948 in estuaries using thymol blue and m-cresol purple, *Mar. Chem.*, 91, 175–186,  
949 doi:10.1016/j.marchem.2004.06.008, 2004.

950 Newcomb, T. W. and Flagg, T. A.: Some effects of Mt. St. Helens volcanic ash on juvenile  
951 salmon smolts., *Mar. Fish. Rev.*, 45(2), 8–12, 1983.

952 Olgun, N., Duggen, S., Croot, P. L., Delmelle, P., Dietze, H., Schacht, U., Óskarsson, N.,  
953 Siebe, C., Auer, A. and Garbe-Schönberg, D.: Surface ocean iron fertilization: The role of  
954 airborne volcanic ash from subduction zone and hot spot volcanoes and related iron fluxes  
955 into the Pacific Ocean, *Global Biogeochem. Cycles*, 25(4), doi:10.1029/2009GB003761,  
956 2011.

957 Olsson, J., Stipp, S. L. S., Dalby, K. N. and Gislason, S. R.: Rapid release of metal salts and  
958 nutrients from the 2011 Grímsvötn, Iceland volcanic ash, *Geochim. Cosmochim. Acta*,  
959 doi:10.1016/j.gca.2013.09.009, 2013.

960 Óskarsson, N.: The interaction between volcanic gases and tephra: Fluorine adhering to  
961 tephra of the 1970 hekla eruption, *J. Volcanol. Geotherm. Res.*, doi:10.1016/0377-  
962 0273(80)90107-9, 1980.

963 Rapp, I., Schlosser, C., Rusiecka, D., Gledhill, M. and Achterberg, E. P.: Automated  
964 preconcentration of Fe, Zn, Cu, Ni, Cd, Pb, Co, and Mn in seawater with analysis using  
965 high-resolution sector field inductively-coupled plasma mass spectrometry, *Anal. Chim.*  
966 *Acta*, 976, 1–13, doi:10.1016/j.aca.2017.05.008, 2017.

967 Reckziegel, F., Bustos, E., Mingari, L., Báez, W., Villarosa, G., Folch, A., Collini, E.,  
968 Viramonte, J., Romero, J. and Osoreo, S.: Forecasting volcanic ash dispersal and coeval  
969 resuspension during the April-May 2015 Calbuco eruption, *J. Volcanol. Geotherm. Res.*,  
970 doi:10.1016/j.jvolgeores.2016.04.033, 2016.

971 Rogan, N., Achterberg, E. P., Le Moigne, F. A. C., Marsay, C. M., Tagliabue, A. and  
972 Williams, R. G.: Volcanic ash as an oceanic iron source and sink, *Geophys. Res. Lett.*,  
973 43(6), 2732–2740, doi:10.1002/2016GL067905, 2016.



974 Romero, J. E., Morgavi, D., Arzilli, F., Daga, R., Caselli, A., Reckziegel, F., Viramonte, J.,  
975 Díaz-Alvarado, J., Polacci, M., Burton, M. and Perugini, D.: Eruption dynamics of the 22–  
976 23 April 2015 Calbuco Volcano (Southern Chile): Analyses of tephra fall deposits, J.  
977 Volcanol. Geotherm. Res., 317, 15–29, doi:10.1016/j.jvolgeores.2016.02.027, 2016.

978 Rubin, C. H., Noji, E. K., Seligman, P. J., Holtz, J. L., Grande, J. and Vittani, F.:  
979 Evaluating a fluorosis hazard after a volcanic eruption, Arch. Environ. Health,  
980 doi:10.1080/00039896.1994.9954992, 1994.

981 Sanchez, N., Bizsel, N., Iriarte, J. L., Olsen, L. M. and Ardelan, M. V.: Iron cycling in a  
982 mesocosm experiment in a north Patagonian fjord: Potential effect of ammonium addition  
983 by salmon aquaculture, Estuar. Coast. Shelf Sci., 220, 209–219,  
984 doi:10.1016/j.ecss.2019.02.044, 2019.

985 Santana-Casiano, J. M., Gonzaalez-Davila, M. and Millero, F. J.: Oxidation of nanomolar  
986 levels of Fe(II) with oxygen in natural waters, Environ. Sci. Technol., 39(7), 2073–2079,  
987 doi:10.1021/es049748y, 2005.

988 Sarmiento, J. L.: Atmospheric CO<sub>2</sub> stalled, Nature, doi:10.1038/365697a0, 1993.

989 Sarthou, G., Bucciarelli, E., Chever, F., Hansard, S. P., Gonzalez-Davila, M., Santana-  
990 Casiano, J. M., Planchon, F. and Speich, S.: Labile Fe(II) concentrations in the Atlantic  
991 sector of the Southern Ocean along a transect from the subtropical domain to the Weddell  
992 Sea Gyre, Biogeosciences, 8(9), 2461–2479, doi:10.5194/bg-8-2461-2011, 2011.

993 Seidel, M. P., DeGrandpre, M. D. and Dickson, A. G.: A sensor for in situ indicator-based  
994 measurements of seawater pH, Mar. Chem., 109(1), 18–28,  
995 doi:10.1016/j.marchem.2007.11.013, 2008.

996 Simonella, L. E., Palomeque, M. E., Croot, P. L., Stein, A., Kupczewski, M., Rosales, A.,  
997 Montes, M. L., Colombo, F., García, M. G., Villarosa, G. and Gaiero, D. M.: Soluble iron

998 inputs to the Southern Ocean through recent andesitic to rhyolitic volcanic ash eruptions  
999 from the Patagonian Andes, *Global Biogeochem. Cycles*, 29(8), 1125–1144,  
1000 doi:10.1002/2015GB005177, 2015.

1001 Siringan, F. P., Racasa, E. D. R., David, C. P. C. and Saban, R. C.: Increase in Dissolved  
1002 Silica of Rivers Due to a Volcanic Eruption in an Estuarine Bay (Sorsogon Bay,  
1003 Philippines), *Estuaries and Coasts*, 41, 2277–2288, doi:10.1007/s12237-018-0428-1, 2018.

1004 Stewart, C., Johnston, D. M., Leonard, G. S., Horwell, C. J., Thordarson, T. and Cronin, S.  
1005 J.: Contamination of water supplies by volcanic ashfall: A literature review and simple  
1006 impact modelling, *J. Volcanol. Geotherm. Res.*, 158(3), 296–306,  
1007 doi:10.1016/j.jvolgeores.2006.07.002, 2006.

1008 Sunda, W. G., Buffle, J. and Van Leeuwen, H. P.: Bioavailability and Bioaccumulation of  
1009 Iron in the Sea, in *The Biogeochemistry of Iron in Seawater*, vol. 7, edited by D. R. Turner  
1010 and K. A. Hunter, pp. 41–84, John Wiley & Sons, Ltd, Chichester., 2001.

1011 Torres, O., Tanskanen, A., Veihelmann, B., Ahn, C., Braak, R., Bhartia, P. K., Veeffkind, P.  
1012 and Levelt, P.: Aerosols and surface UV products from Ozone Monitoring Instrument  
1013 observations: An overview, *J. Geophys. Res. Atmos.*, doi:10.1029/2007JD008809, 2007.

1014 Torres, R. and Ampuero, P.: Strong CO<sub>2</sub> outgassing from high nutrient low chlorophyll  
1015 coastal waters off central Chile (30°S): The role of dissolved iron, *Estuar. Coast. Shelf Sci.*,  
1016 83(2), 126–132, doi:10.1016/j.ecss.2009.02.030, 2009.

1017 Torres, R., Silva, N., Reid, B. and Frangopulos, M.: Silicic acid enrichment of subantarctic  
1018 surface water from continental inputs along the Patagonian archipelago interior sea (41-  
1019 56°S), *Prog. Oceanogr.*, 129, 50–61, doi:10.1016/j.pocean.2014.09.008, 2014.

1020 Utermöhl, H.: Zur Vervollkommnung der quantitativen Phytoplankton-Methodik, *SIL*  
1021 *Commun.* 1953-1996, doi:10.1080/05384680.1958.11904091, 1958.

1022 Vergara-Jara, M. J., DeGrandpre, M. D., Torres, R., Beatty, C. M., Cuevas, L. A., Alarcón,  
1023 E. and Iriarte, J. L.: Seasonal Changes in Carbonate Saturation State and Air-Sea CO<sub>2</sub>  
1024 Fluxes During an Annual Cycle in a Stratified-Temperate Fjord (Reloncaví Fjord, Chilean  
1025 Patagonia), *J. Geophys. Res. Biogeosciences*, 124(9), 2851–2865,  
1026 doi:10.1029/2019JG005028, 2019.

1027 Watson, A. J.: Volcanic iron, CO<sub>2</sub>, ocean productivity and climate, *Nature*,  
1028 doi:10.1038/385587b0, 1997.

1029 Weinbauer, M. G., Guinot, B., Migon, C., Malfatti, F. and Mari, X.: Skyfall - neglected  
1030 roles of volcano ash and black carbon rich aerosols for microbial plankton in the ocean, *J.*  
1031 *Plankton Res.*, 39(2), 187–198, doi:10.1093/plankt/fbw100, 2017.

1032 Welschmeyer, N. A.: Fluorometric analysis of chlorophyll a in the presence of chlorophyll  
1033 b and pheopigments, *Limnol. Oceanogr.*, doi:10.4319/lo.1994.39.8.1985, 1994.

1034 Witham, C. S., Oppenheimer, C. and Horwell, C. J.: Volcanic ash-leachates: a review and  
1035 recommendations for sampling methods, *J. Volcanol. Geotherm. Res.*, 141(3), 299–326,  
1036 doi:10.1016/j.jvolgeores.2004.11.010, 2005.

1037 Wolinski, L., Laspoumaderes, C., Bastidas Navarro, M., Modenutti, B. and Balseiro, E.:  
1038 The susceptibility of cladocerans in North Andean Patagonian lakes to volcanic ashes,  
1039 *Freshw. Biol.*, 58, 1878–1888, doi:10.1111/fwb.12176, 2013.

1040 Yevenes, M. A., Lagos, N. A., Farías, L. and Vargas, C. A.: Greenhouse gases, nutrients  
1041 and the carbonate system in the Reloncaví Fjord (Northern Chilean Patagonia):  
1042 Implications on aquaculture of the mussel, *Mytilus chilensis*, during an episodic volcanic  
1043 eruption, *Sci. Total Environ.*, doi:10.1016/j.scitotenv.2019.03.037, 2019.

1044